Received: 25 July 2018 | Revised: 1 September 2018 | Accepted: 3 September 2018
DOI: 10.1002/aoc.4611

FULL PAPER

WILEY Applied Organometallic Chemistry

Experimental and computational exploration of photophysical and electroluminescent properties of modified 2,2′:6′,2″-terpyridine, 2,6-di(thiazol-2-yl)pyridine and 2,6-di(pyrazin-2-yl)pyridine ligands and their Re(I) complexes

Tomasz Klemens[1] | Anna Świtlicka[1] | Agata Szlapa-Kula[1] | Stanisław Krompiec[1] | Piotr Lodowski[1] | Anna Chrobok[3] | Magdalena Godlewska[4] | Sonia Kotowicz[1] | Mariola Siwy[2] | Katarzyna Bednarczyk[1] | Marcin Libera[1] | Sebastian Maćkowski[5] | Tomasz Pędziński[6] | Ewa Schab-Balcerzak[1,2] | Barbara Machura[1]

[1] Institute of Chemistry, University of Silesia, 9 Szkolna Str., 40-006 Katowice, Poland

[2] Centre of Polymer and Carbon Materials, Polish Academy of Sciences, 34 M. Curie-Sklodowska Str., 41-819 Zabrze, Poland

[3] Faculty of Chemistry, Silesian University of Technology, 9 Strzody Str., 44-100 Gliwice, Poland

[4] Mass Spectrometry Group, Institute of Organic Chemistry, Polish Academy of Sciences, Kasprzaka 44/52, PO Box 58, 01-224 Warszawa, Poland

[5] Institute of Physics, Faculty of Physics, Astronomy and Informatics, Nicolaus Copernicus University, 5 Grudziądzka Str., 87-100 Torun, Poland

[6] Faculty of Chemistry, Adam Mickiewicz University in Poznań, 89b Umultowska, 61-614 Poznań, Poland

Correspondence
Schab-Balcerzak and Barbara Machura, Institute of Chemistry, University of Silesia 9 Szkolna Str., 40-006 Katowice, Poland.
Email: ewa.schab-balcerzak@us.edu.pl; barbara.machura@us.edu.pl

Funding information
Narodowe Centrum Nauki, Grant/Award Number: DEC-2017/25/B/ST5/01611

The excited-state characteristics of a series of 2,2′:6′,2″-terpyridine (terpy), 2,6-di(thiazol-2-yl)pyridine (dtpy) and 2,6-di(pyrazin-2-yl)pyridine (dppy) derivatives as well as their corresponding Re(I) complexes [ReCl(CO)$_3$(L^n-κ^2N)] were investigated both experimentally and theoretically, and the crucial effect of pyrrolidine substituent and peripheral rings on the optical and electrochemical properties was found evident. For Re(I) complexes bearing the ligands with electron-rich pyrrolidine substituent, different emission profiles were found in polar and non-polar solvents, indicating a change in the character of the excited state. Dual-emission effect of [ReCl(CO)$_3$(L^4-κ^2N)] and [ReCl(CO)$_3$(L^5-κ^2N)] in chloroform was attributed to the presence of two emitting states, identified as an ^{1}ILCT excited state deactivated at higher energies and a longer-lived red-shifted phosphorescence assigned to the ^{3}MLCT excited state. The triplet excited state was confirmed by recording the nanosecond time-resolved transient absorption spectra for the compound [ReCl(CO)$_3$(L^4-κ^2N)]. To verify the charge transfer problem of low-lying excited states of the free ligands, the Λ parameter was calculated. In addition, the compounds were applied as emitting layers for both non-doped and doped single-layer organic light-emitting diodes fabricated by solution processing.

KEYWORDS
donor–acceptor ligands, electroluminescence, OLEDs, photoluminescence, Re(I) complexes

1 | INTRODUCTION

The photophysical properties of Re(I) tricarbonyl complexes with diimine ligands have been the focus of numerous investigations[1] since 1974, when unusual excited-state properties of $[ReCl(CO)_3(4,7\text{-}(Ph)_2phen)]$ and $[ReCl(CO)_3(5\text{-}R\text{-}phen)]$ were discovered by Wrighton and Morse.[2] The development of this area is driven not only by intriguing photophysical features, but chiefly by high potential of $[ReL(CO)_3(N^\cap N)]^{n+}$ ($n = 0$ or 1) to serve as catalysts,[3] multimodal platforms for inorganic chemical biology,[4] sensors,[5] promising molecular switches[6] and organic light-emitting device emitters.[7]

For the majority of these complexes, photoexcitation involves metal-to-ligand charge transfer (MLCT) or mixed MLCT/ligand-to-ligand charge transfer (frequently denoted as MLLCT) type transitions, where the frontier orbitals are considerably delocalized over both the ligand(s) and the metal centre. It has been demonstrated that the energies of the metal-based d_π and diimine-based π^*, which act as the electron donor and acceptor in MLCT transitions, can be fine-tuned by introduction of electron-withdrawing or electron-donating groups into diamine ligand skeleton ($N^\cap N$) or changing the ancillary ligand (L).[1,8]

In recent years, special attention has been paid to strong electron-donating substituents, such as triarylamines and thioethers, which – when introduced into a diamine skeleton – can give rise to intraligand charge transfer (ILCT) transitions from donor orbital localized on the electron-rich group to diimine-based π^*acceptor orbital. Compared to the conventional MLCT excitations, they have higher extinction coefficients and they are characterized with lower energies.[9]

ILCT transitions were found to govern spectral properties of Re(I) carbonyls with sulfur- and triarylamine-substituted dipyridophenazine,[10] 1,10-phenanthroline functionalized by carbazole group[11] and triphenylamine-substituted 1,10-phenanthroline and 2-pyridyl-1,2,3-triazole.[12] For *fac*-$[Re(L)(CO)_3(cbz_2phen)]^{+/0}$ (cbz_2phen = 4,7-di(9H-carbazol-9-yl)-1,10-phenanthroline and L = Cl $^-$, pyridine or 2-aminomethylpyridine), solution-phase time-resolved photoluminescence (PL) confirmed the presence of two emitting states, identified as $^1ILCTc_{bz2phen}$ excited state deactivation at higher energies and a long-lived phosphorescence attributed to the $^3MLCT_{Re\rightarrow cbz2phen}$ excited state.[5,11] Dual charge transfer has been also confirmed in Re(I) thioether substituted hexaazanaphthalene complexes.[13] It is assumed that photoexcitation of these systems can optically populate both ligand-centred $^1\pi\pi^*$ and ^{1}MLCT states, which can potentially relax via independent pathways.[14] Coexistence of the distinct excited states offers additional opportunity for fine-tuning the luminescent properties of this class of compounds. Most importantly, the use of highly emitting neutral tricarbonyl Re(I) complexes with donor–acceptor characteristics, such as $[ReBr(CO)_3(PTIP)]$, $[ReBr(CO)_3(TPIP)]$ and $[ReBr\ (CO)_3(TTIP)]$ (PTIP = *N*,*N*-diphenyl- 4-(1-phenyl-1*H*-imidazo[4,5-*f*][1,10]phenanthrolin-2-yl)aniline, TPIP = *N*, *N*-diphenyl-4-(2-phenyl-1*H*-imidazo[4,5-*f*][1,10]phenanthrolin-1-yl)aniline, TTIP = 4,40-(1*H*-imidazo[4,5-*f*][1,10] phenanthroline-1,2-diyl)bis(*N*,*N*-diphenylaniline)), as doped emitters in organic light-emitting diodes (OLEDs) allowed the achievement of remarkable device performances.[7e]

In an attempt to further understand the effect of strong electron-releasing substituents, a series of Re(I) carbonyls with modified 2,2′:6′,2″-terpyridine (terpy), 2,6-di(thiazol-2-yl)pyridine (dtpy) and 2,6-di(pyrazin-2-yl)pyridine (dppy) ligands (Scheme 1) have been synthesized and the nature and energies of the electronic transitions that occur in these systems were investigated both experimentally (with UV–visible absorption and emission spectroscopies) and theoretically (using density functional theory (DFT) calculations at the PBE1PBE/DEF2–TZVPD/DEF2-TZVP

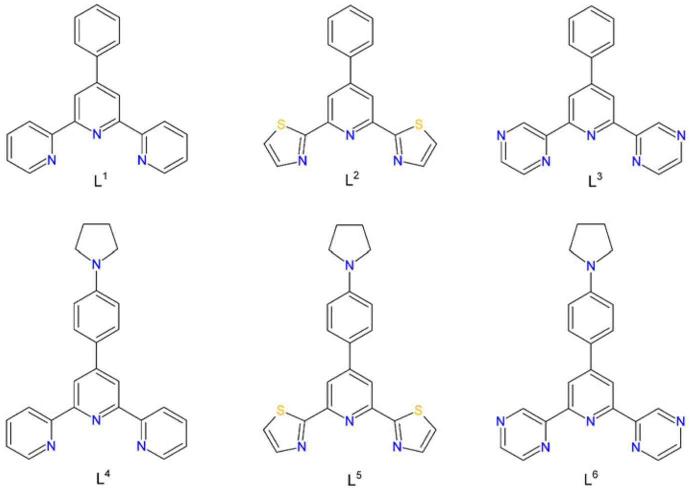

SCHEME 1 Ligands employed in this study.

level). Phenyl-substituted triimine ligands (L^1–L^3) and their Re(I) complexes [$ReCl(CO)_3(L^n$-$\kappa^2N)$] (**1–3**) were synthesized as control compounds, to get a better understanding of ILCT transitions in the systems with electron-rich pyrrolidine group (L^4–L^6 and **4–6**). To further modulate both donor–acceptor and photopysical properties of L^1–L^6 and **1–6**, three different triimine skeletons (terpy, dtpy and dppy) were used.

In addition, the obtained compounds were characterized using electroluminescence (EL), and some of them were applied as emitting layers for both non-doped and doped single-layer OLEDs fabricated by solution processing.

2 | RESULTS AND DISCUSSION

2.1 | Synthesis and General Characterization

Derivatives of terpy, dtpy and dppy were obtained by condensation of the corresponding aldehyde with 2-acetylpyridine, 2-acetylthiazole and 2-acetylpyrazine, respectively (Fig. S1 in supporting information). The products of the base-mediated Kröhnke condensation were not isolated, but underwent *in situ* pyridine ring closure in the presence of an ammonia source.[15]

The complexes **1–6** were isolated as orange (**1**, **4**, **5**), yellow (**2**, **3**) and red (**6**) solids by reaction of [$Re(CO)_5Cl$] with one equivalent of the corresponding ligand in acetonitrile at refluxing temperature.

The infrared (IR) spectra of **1–6** display two overlapping lower energy bands (1932–1876 cm^{-1}) and sharp intense bands at higher wavenumbers (2030–2018 cm^{-1}) attributed to $\nu(C\equiv O)$ of the *fac*-[$Re(CO)_3]^+$ moiety. The medium intensity stretching modes ν(CN) and $\nu(C{=}C)$ of the organic ligand L^n (n = 1–6) occur in the range 1615–1526 cm^{-1} (Fig. S2 in supporting information). Consistent with the bidentate coordination mode of L^n, the resonances attributed to the outer piryd-2-yl/thiazol-2-yl/pyrazin-2-yl protons are clearly differentiated in ^1H NMR spectra (Fig. S3 in supporting information). Distinctive signals corresponding to the carbonyl groups appear at 198 and 190 ppm in ^{13}C NMR spectra.

Solubility tests of the synthesized compounds were carried out in chloroform to determine whether the studied ligands and complexes reach a concentration of 10 mg ml^{-1}, used in the procedure of layer formation (see Section 4). It was found that compounds with the pyrrolidine substituent and without pyrazine ring were fully soluble, whereas molecules without pyrrolidine unit (L^1–L^3 and **1–3**) or with pyrazine ring (L^6 and **6**) were only partially dissolved. It can be concluded that the presence of pyrrolidine substituent attached to the phenyl group enhances the solubility, while the introduction of pyrazine ring leads to its reduction.

2.2 | X-ray Structures

The complexes **1–6** show a distorted octahedral geometry around the central Re(1) atom, with three *fac*-disposed carbonyl ligands, chloride ion and two nitrogen atoms of the organic ligand L^n – one from the central pyridine and one from the peripheral ring (pyridine in L^1 and L^4, thiazole in L^2 and L^5 and pyrazine in L^3 and L^6) (Fig. 1 and Fig. S9). The uncoordinated pyrid-2-yl in **1** and **4**, thiazol-2-yl in **2** and **5** and pyrazin-2-yl in **3** and **6** interact sterically with the carbonyl group C(1)–O(1), which is manifested in a significant increase of C(1)–Re(1)–N(2) angle (101.70(2)° in **1**, 102.2(3)° in **2**, 100.27(19)° in **3**, 102.70(17)° in **4**, 100.40(18)° in **5**, 103.36(16)° in **6**), being the largest one between any two *cis*-arranged ligands in [$ReCl(CO)_3(L^n$-$\kappa^2N)$] (Table S1). Typically for Re(I) complexes incorporating bidentate-coordinated conjugated triimine ligands, the Re(1)–N(2) bond length to the

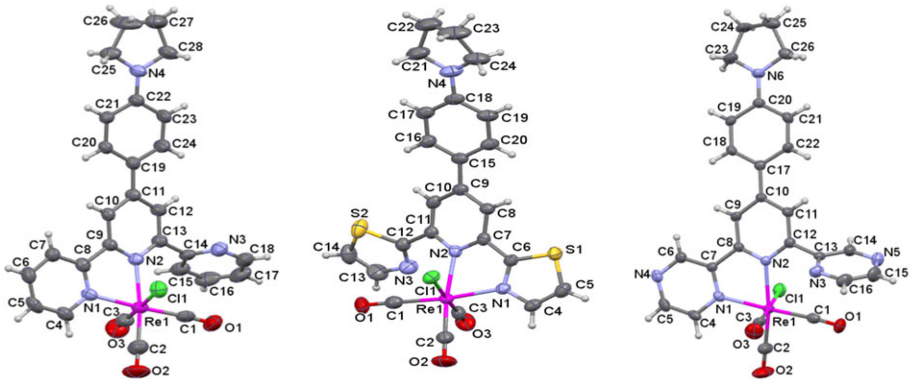

4 **5** **6**

FIGURE 1 Perspective views demonstrating the molecular structures of **4**, **5** and **6** with atom numbering. Atomic displacement ellipsoids are drawn at the 50% probability level.

central pyridine (2.223(5) Å in **1**, 2.244(6) Å in **2**, 2.198(4) Å in **3**, 2.204(4) Å in **4**, 2.236(4) Å in **5**, 2.213(3) Å in **6**) is longer than the corresponding Re(1)–N(1) distance to the pyrid-2-yl/thiazol-2-yl/pyrazin-2-yl ring (2.179(5) Å in **1**, 2.157(5) Å in **2**, 2.160(4) Å in **3**, 2.170(3) Å in **4**, 2.151(4) Å in **5**, 2.159(4) Å in **6**). To a large extent, the angular distortion of **1–6** from the ideal octahedral geometry is attributed to the occurrence of five-member chelate ring of L^n resulting in N(2)–Re(1)–N(1) angle of 74.58(17)° for **1**, 74.9(2)° for **2**, 74.42(14)° for **3**, 74.25(13)° for **4**, 74.11(14) for **5**, 74.22(12)° for **6** (Table S1), significantly smaller than the ideal 90° angle of an octahedron. The coordinated peripheral ring is almost coplanar with the central pyridine ring, with a dihedral angle of 13.43° in **1**, 2.37° in **2**, 11.35° in **3**, 8.71° in **4**, 15.09° in **5**, 10.56° in **6**, while the uncoordinated piryd-2-yl/thiazol-2-yl/pyrazin-2-yl rings are inclined to the central pyridine at 50.18° in **1**, 59.28° in **2**, 48.21° in **3**, 64.00° in **4**, 33.36° in **5**, 61.48° in **6**. The dihedral angles between the least squares planes of the pyridine and phenyl rings are 11.15° in **1**, 6.63° in **2**, 17.71° in **3**, 13.87° in **4**, 17.67° in **5**, 13.99° in **6**.

To explore the impact of the triimine modification on the local geometry, the sum of bond angles around the Re(I) centre has also been calculated. For structures **1–6**, the calculated values of 1604.11°, 1596.78°, 1600.37°, 1602.67°, 1599.47° and 1603.56°, slightly lower than the 1620° for an ideal octahedral ligand arrangement,[16] are comparable to each other and indicate a negligible effect of the pyrrolidine substituent and peripheral rings of L^n on the local geometry around the rhenium centre.

A summary of the intermolecular contacts in the crystal structures of **1–6** is provided in spots of Hirshfeld surfaces mapped with d_{norm} and in two-dimensional fingerprint plots (Fig. S10 in supporting information). The relative contributions of various intermolecular interactions to the Hirshfeld surfaces are illustrated in Fig. 2. As shown in Fig. 2 and Fig. S10 (supporting information), weak hydrogen bonds C—H⋯O, C—H⋯Cl or C—H⋯S are dominant in the examined crystal structures. For **1** and **3**, also contribution of π-stacking was evident (see also Table S3).

2.3 | Differential Scanning Calorimetry and Thermogravimetric Analysis

Temperature stability of compounds incorporated in OLED structures is required to sustain continuous Joule heating when the voltage is applied and the resulting possible thermal breakdown. It was found that local heating in a current-driven organic device may lead to localized electrical shortcuts, which raised the temperature to 180–200°C within a device.[17] The thermal properties of the free ligands L^1–L^6 and complexes **1–6** were measured using differential scanning calorimetry and thermogravimetric analysis under nitrogen atmosphere and the data are collected in Table S5, while representative differential scanning calorimetry curves of this family of compounds can be found in the supporting information (Fig. S11).

Considering the effect of the pyrrolidine substituent attached to the phenyl group, it can be concluded that introduction of such a unit slightly affects the melting temperature (T_m). However, the presence of pyrrolidine gives the possibility of generating an amorphous phase, and, in the second heating scan, after rapid cooling, the glass transition (T_g) was observed. The presence of pyrazine rings in ligands L^3 and L^6 increases both T_m and T_g values. All of the complexes exhibited higher T_m with respect to the corresponding ligands. The complexes melted with decomposition except for **3** and **5**. Thermal decomposition of the ligands, in contrast to the complexes, proceeded in a single step. The temperature of 5% weight loss (T_5), taken as the beginning of decomposition, was also higher for the Re(I) complexes. It can be concluded that these compounds have good thermal stability with T_5 in the range 221–350°C.

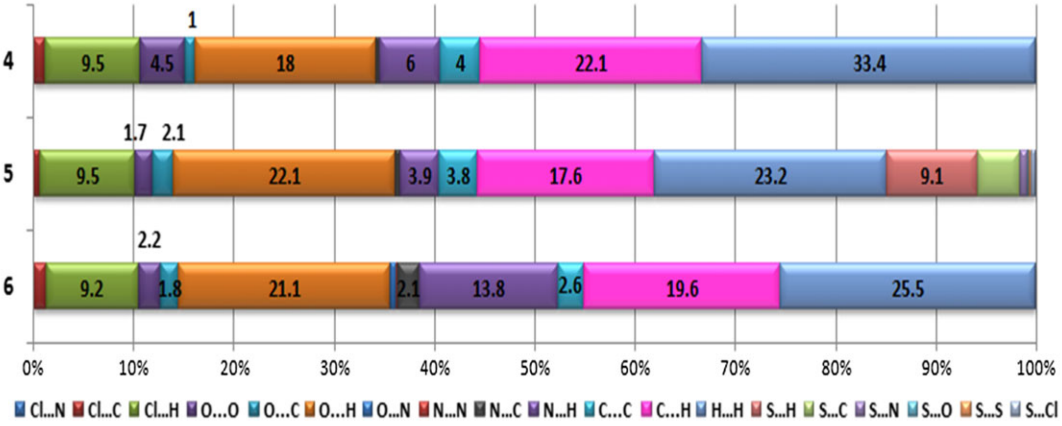

FIGURE 2 Relative contributions of various intermolecular interactions to the Hirshfeld surfaces for complexes **4–6**.

2.4 | Electrochemistry

The redox potentials of the free ligands L^1–L^6 and complexes **1–6** were measured using cyclic voltammetry and differential pulse voltammetry in MeCN with the aid of 0.1 M Bu_4NPF_6 as the supporting electrolyte. The results are summarized in Table S6. The onsets of the first oxidation and reduction peak were used to estimate the ionization potentials (IP) and the electron affinities (EA), assuming IP of ferrocene to be equal to −5.1 eV.[18]

The voltammograms of the free ligands display one or two reduction processes in the negative potential range. The first reversible reduction potentials were found to be unaffected by introduction of the pyrrolidine substituent into triimine ligand. The reduction of L^4–L^6 occurs at potentials similar to those for the corresponding L^1–L^3, which implies that the LUMOs of the ligands are dominated by the contributions of π^* orbitals of terpy, dtpy and dppy skeleton. This conclusion is supported by the fact that the reduction potentials of L^1–L^6 are sensitive to the peripheral rings of the heterocyclic systems. As shown by the data summarized in Table S6, the more negative reduction potentials are reported for terpy derivatives (L^1 and L^4). Thus, π-acceptor capability of the studied triimine ligands is improved by the inclusion of thiazole and pyrazine rings. For the Re(I) complexes, the reduction peaks were found at more positive values compared to the corresponding ligands, and the first reversible reduction potentials of **1–6** are influenced by both peripheral rings and pyrrolidine substituent of the ligand L^n. The complexes bearing the pyrrolidine moiety display more negative reduction potentials in relation to the corresponding **1**, **2** and **3**, which can be attributed to electron-donor effect induced by the pyrrolidine group. For both series of compounds, L^1–L^3 and L^4–L^6, the first reduction potentials have become more positive in the order pyridine < thiazole < pyrazine, consistent with the trend observed for the free ligands. This corresponds to lowering the LUMO levels in both series **1–3** and **4–6** (Fig. 3).

The first oxidation potentials of the Re(I) complexes bearing the pyrrolidine moiety (**4–6**) were found at very low values. These values are insensitive to the peripheral rings and they all fall in the range observed for the free ligands L^4–L^6. Most probably, the oxidation process in L^4–L^6 and **4–6** is associated with oxidation of the pyrrolidine moiety itself, and the HOMO of these systems is chiefly influenced by the N-donor substituent. With reference to previous studies,[19] the redox waves at more positive potentials, for both **1–3** and **4–6**, can be assigned to the metal-centred Re(I/II) oxidation process.

The electrochemical band gaps E_g are in satisfactory agreement with the optical band gaps E_g^{opt}, but, more importantly, all the examined Re(I) complexes exhibited values of E_g that make them potentially useful for optoelectronic applications.

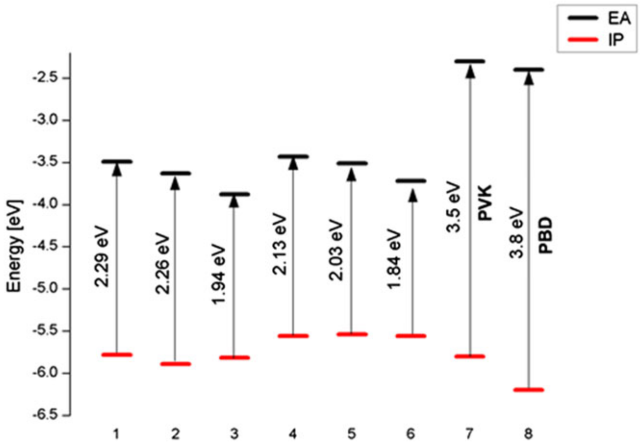

FIGURE 3 HOMO and LUMO energy levels for PVK (as **7**), PBD (as **8**) and IP and EA of synthesized compounds with respect to the vacuum level.

2.5 | UV–Visible Absorption Spectroscopy

The electronic absorption spectra of L^1–L^6 show a collection of bands in the range 374–191 nm. The position of the lowest-energy band (at 374–309 nm) is unaffected by changes in solvent polarity (Table S7; Figs S12 and S13), indicating that the ground and excited states have similar dipole moments. Of note, the introduction of electron-donating pyrrolidine substituent results in significant red shift and intensity increase of the lowest energy band. The longest wavelength absorption peak of L^4–L^6 appeared at wavelengths more than 20 nm longer with respect to that recorded for the ligands L^1–L^3, and its absorption coefficient is more than twice larger. This enhanced and red-shifted absorption of L^4–L^6 can be attributed to excitation leading to the formation of an intramolecular charge transfer (ICT) state, which is a result of charge delocalization from the pyrrolidine donor unit to π-conjugated triimine acceptor moiety. Due to strong electron-donating properties of pyrrolidine substituent, the HOMO orbital of L^4–L^6 is expected to rise higher in energy compared to L^1–L^3, which leads to the shrinking of the HOMO–LUMO energy gap and a red shift in absorption spectra. The location of the lowest energy absorption band of the free ligands is also sensitive to the donor–acceptor properties of the peripheral rings: pyridine in L^1 and L^4, thiazole in L^2 and L^5 and pyrazine in L^3 and L^6. For both series, L^1–L^3 and L^4–L^6, the red shift was in the order thiazole > pyrazine > pyridine.

Upon formation of **1–6**, the spin-allowed intraligand transitions of the substituted terpy, dtpy and dppy ligands are slightly red-shifted (falling in the range 200–375 nm) and an additional absorption emerges in the visible part of each spectrum (Table S7 and Fig. 4a). Of note, the lowest-energy band of **4**, **5** and **6** has a significantly higher extinction coefficient and it is red-shifted by 24–50 nm in comparison with **1**, **2** and **3**, respectively (Fig. 4b). These variations in absorption characteristics may indicate changes in the character of the electronic transitions: ^{1}MLCT arising from the d_π (Re) → π^*_L transitions for **1**–**3**[8b,c,e,h–k] and ^{1}ILCT originating from charge transfer from the pyrrolidine donor to π-conjugated triimine acceptor for **4**–**6**.[20] Such an assignment is consistent with the electrochemical data indicating that the first oxidation for **4**–**6** is centred at the pyrrolidine unit as well as being supported by theoretical calculations (see Section 2.9). Nevertheless, due to some overlap of MLCT and ILCT transitions, it is not possible to completely exclude the participation of $Re_d \rightarrow \pi^*_{triimine}$ excitations in the lowest energy band of **4**–**6**.

As evident from Table S7 and shown in Fig. 4, the energies of MLCT bands for **1**–**3** and ILCT bands for **4**–**6** are influenced by acceptor properties of the peripheral rings of the triimine skeleton (pyridine in **1** and **4**, thiazole in **2** and **5** and pyrazine in **3** and **6**). For both **1**–**3** and **4**–**6**, the red shift was in the order pyrazine > thiazole > pyridine, which implies the strongest electron-withdrawing properties for compounds bearing dppy ligands.

Expectedly for charge transfer bands, the position of the lowest energy absorption of **1**–**6** is affected by changes in solvent polarity. On passing from acetonitrile to chloroform solution, the longest wavelength absorption band of the complexes is red-shifted by 22.5 nm for **1**, 28.8 nm for **2**, 26.4 nm for **3**, 6.8 nm for **4**, 10.7 nm for **5** and 15.9 nm for **6**. In addition, the UV–visible spectra for selected compounds (L^1, L^4, L^5, **1**, **4** and **5**) as thin films on a glass substrate were recorded. In the case of the ligands, the position of maximum absorption band (λ_{max}) in the solid state was bathochromically shifted with respect to the solution phase (cf. Fig. S14). Such a shift of λ_{max} is noted for various compounds and it can be explained by 'J' type aggregation, which takes place when molecules stack in a head-to-tail arrangement.[21] The first absorption band in UV–visible spectra of Re(I) complexes in film is slightly shifted to higher energy spectral range compared to the chloroform solution (cf. Fig. S14 and Table S7).

2.6 | Photoluminescence

A summary of the photophysical data for L^1–L^6 and **1**–**6** is given in Tables S8 and S9, respectively, and the normalized excitation spectra, emission spectra and decay curves are shown in Fig. S15 in supporting information.

In solution, the free ligands L^1–L^3 exhibited weak or moderate emission in the near-UV region of 340–400 nm (Fig. S16). Fluorescence of the ligands bearing electron-rich pyrrolidine substituent (L^4–L^6) appeared in a significantly lower energy region (462–645 nm). There is also a marked difference in the fluorescence maximum wavelength depending on the electronic properties of the peripheral rings of the triimine ligands. The wavelength of the ligand emission is significantly red-shifted in the orders $L^3 > L^2 > L^1$ and $L^6 > L^5 > L^4$.

In contrast to L^1–L^3, the fluorescence maximum wavelength of the ligands containing pendant amine group (L^4–L^6) is strongly dependent on the solvent polarity. On passing from chloroform to acetonitrile, the emission of L^4, L^5 and L^6 shifted by 74, 105 and 123 nm towards longer wavelengths, respectively. Positive solvatochromism, which indicates better stabilization of the excited state in more polar solvents, is expected for ICT transitions. To further evaluate the ICT character of the excited state in the case of L^4–L^6, the difference between the excited and ground state dipole moments ($\Delta\mu = \mu_e - \mu_g$) was estimated using the Lippert–Mataga equation (equation (1)):

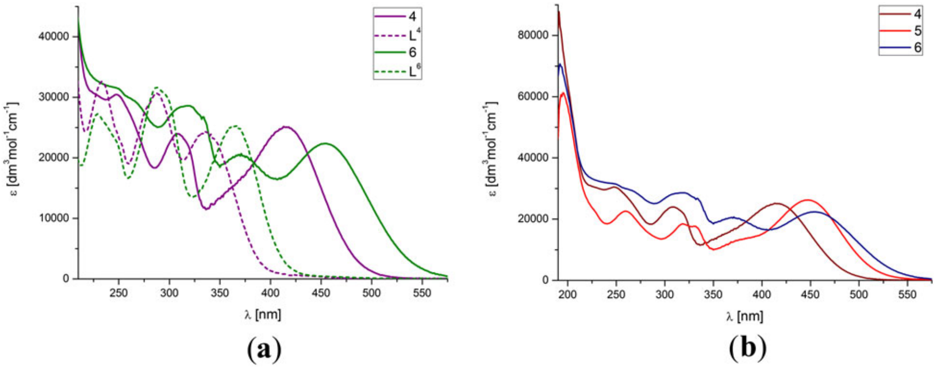

(a) (b)

FIGURE 4 (a) UV–visible spectra of ligands and Re(I) complexes in MeCN demonstrating the impact of pyrrolidine substituent. (b) UV–visible spectra of Re(I) complexes in MeCN demonstrating the impact of peripheral rings.

$$\Delta E_{\text{exc-em}} = \frac{2\left(\mu_e - \mu_g\right)^2}{hca^3}\Delta f + \text{const.} \tag{1}$$

$$\Delta f = \frac{\varepsilon - 1}{2\varepsilon + 1} - \frac{n^2 - 1}{2n^2 + 1} \tag{2}$$

where $\Delta E_{\text{exc-em}}$ is the Stokes shift (cm^{-1}), h is Planck's constant, c is the speed of light in vacuum, a is the Onsager cavity radius and Δf is the orientation polarizability of the solvent, which measures both electron mobility and dipole moment of the solvent molecule. Δf was calculated using equation (2), where ε is the dielectric constant of the solvent and n the optical refractive index of the solvent. Onsager cavity radii (a) were calculated theoretically with use of Gaussian09[22] and are collected in Table S10 in supporting information. The structured profile of the emission of the ligands bearing electron-rich pyrrolidine substituent (Fig. 5) may be attributed to locally excited terpy-, dtpy- and dppy-centred $\pi \rightarrow \pi^*$ transitions, which lack the charge transfer character. With increased solvent polarity, the vibronic structure of emission spectra turned to broad unstructured profile, suggesting a conversion from locally excited to ICT state. The large values of $\Delta\mu$ (21.4, 23.1 and 21.8 D for L^4, L^5 and L^6, respectively) estimated by fitting the emission data to the Lippert–Mataga equation imply a dominant contribution of ICT character in the excited state.[23]

Measurements of the PL emission quantum yields revealed a marked decrease in the fluorescence yield of L^4–L^6 with increasing polarity, which is supportive for acceleration of ICT → TICT. The formation of a TICT state leads to orbitally decoupled π systems of the donor and acceptor units with forbidden radiative transition to the ground state, and thus small fluorescence quantum yield.[24] The most considerable decrease was observed for compound L^6, and its quantum efficiency in MeCN is *ca* 20 times lower compared to chloroform. Expectedly, fluorescence quantum yields of L^1–L^6 are strongly dependent on their own molecular structure. The attachment of pyrrolidine to the phenyl ring of terpy and dppy derivatives resulted in a significant increase in the fluorescence quantum yield. On the contrary, a marked drop in fluorescence quantum yields is seen upon replacing the pyridine peripheral ring (L^1 and L^4) by pyrazine (L^3 and L^6). All the ligands reported here were also found to be emissive in the solid state, and stronger emissive properties were found for the ligands bearing the electron-rich pyrrolidine moiety, except for dtpy derivatives. Investigation of effect of excitation wavelength (λ_{ex}) on PL of the ligands in film showed that the highest PL intensity was recorded under λ_{ex} = 310 nm for L^1–$L^3$and L^6 or 330 nm for L^4 and L^5 (cf. Fig. S17). The compounds with pyrrolidine substituent (L^4–L^6) as powder and in the form of a layer on a glass substrate exhibited green fluorescence, while the fluorescence of L^1–L^3 was generally located in near-UV or blue spectral regions (Fig. S16). The presence of two bands in the case of L^2 and L^3 may be attributed to coexistence of monomer and excimer-like emissions.[25] Except for L^6, the maximum of the emission band (λ_{em}) of the ligands in the form of a layer on a glass substrate was bathochromically shifted with respect to the solution phase (in $CHCl_3$) (cf. Fig. S18a,b). In the case of the ligands without pyrrolidine substituent (L^1–L^3), the red shift is rather small and falls in the range 10–19 nm. More pronounced shift, of about 70 nm, was observed in the PL spectra of the ligands bearing pyrrolidine unit (L^4 and L^5). Such a shift may indicate, among others, the contribution

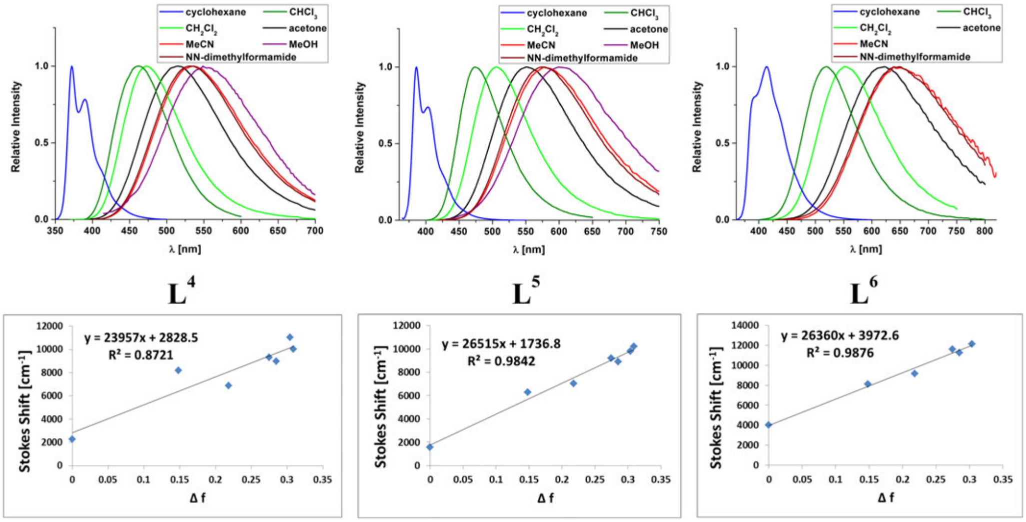

FIGURE 5 Emission spectra of ligands L^4–L^6 in various solvents with Lippert–Mataga plots.

of ILCT transitions and the presence of strong excited-state interactions between the neighbouring molecules. In PL spectra of the ligands dispersed in a poly(9-vinylcarbazole) (PVK):2-(4-*tert*-butylphenyl)-5-(4-biphenylyl)-1,3,4-oxadiazole (PBD) matrix, an emission band with λ_{em} located in the range from 395 to 442 nm was observed. Noteworthy, the emission of ligands L^1–L^4 corresponded to matrix emission (cf. Fig. S18a,b). In the case of compounds L^5 and L^6 in matrix, λ_{em} was bathochromically shifted with respect to λ_{em} of PVK: PBD (cf. Fig. S18a,b).

Excitation of **1–6** in solution at the lowest absorption band gave rise to an emission band with a maximum located in the red spectral region. The decrease in luminescence intensity compared to the free ligands can be explained by the smaller energy gap and faster non-radiative decay according to the energy gap law. According to the data summarized in Table S9, different emission properties were found for series **1–3** and **4–6**. Most importantly, the complexes bearing the triimine ligands with pyrrolidine substituent exhibited different emission profiles in polar acetonitrile and non-polar chloroform, which may indicate changes in the nature of the excited states depending on solvent polarity. For complexes **1–6** being MLCT emitters, the incorporation of the pyrolidine group, which act as electron-donating substituent, is expected to destabilize the MLCT excited state leading to hypsochromic shifts of emission in relation to the parent Re(I) complexes – not having electron-rich moiety attached to the ligand L. This trend was seen in non-polar chloroform for **4–6** in relation to complexes **1–3** being pure MLCT emitters. Of note, the emission spectra of **4** and **5** in $CHCl_3$ exhibited two well-separated bands, at 507 and 677 nm for **4** and 536 and 686 nm for **5**. For both compounds, the intensity of the short-wavelength emission decreased with increasing excitation wavelengths (Fig. 6). In analogy to the previously reported Re(I) polypyridyl compounds *fac*-$[Re(L)(CO)_3(cbz_2phen)]^{+/0}$, where cbz_2phen = 4,7-di(9H-carbazol-9-yl)-1,10-phenanthroline and L = Cl^-, pyridine or 2-aminomethylpyridine,[8h] it can be speculated that the two emission bands of **4** and **5** originate from different excited states. The higher energy band of **4** and **5** is suggested to be of singlet origin and ILCT character. The strong electron-donating property of the pyrrolidine substituent gives rise to an ILCT transition from the pyrrolidine donating group to the terpy accepting moiety (see Section 2.9). Compared to the free ligands, these bands are red-shifted by 45 nm for **4** and 61 nm for **5**, which is attributed to the impact of the metal centre. The broader lower energy emission peak of **4** and **5**, associated with a longer lifetime, is proposed to be of triplet MLCT origin.

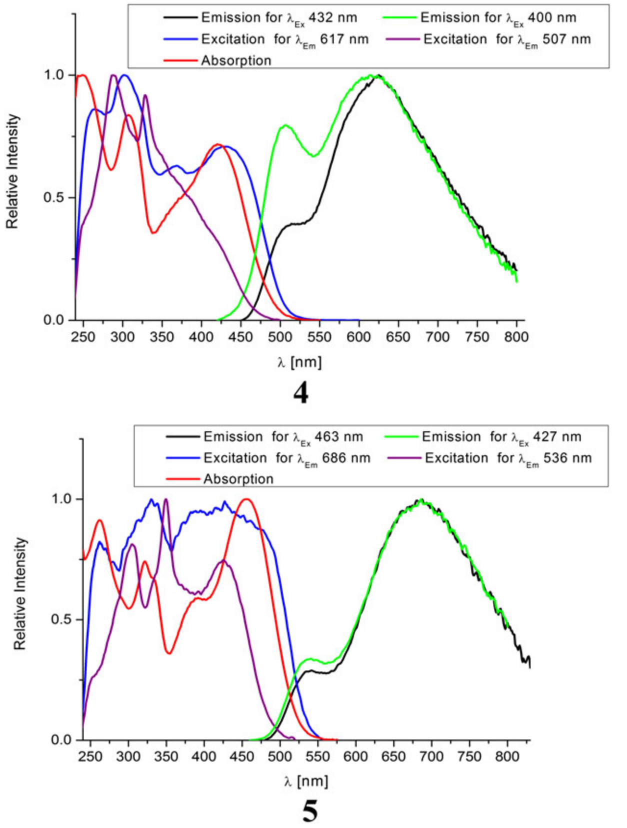

4

5

FIGURE 6 Excitation, emission and absorption of complexes **4** and **5** in $CHCl_3$.

For complex **6**, excitation at the lowest absorption band gave rise to one structureless emission band with a maximum at 690 nm. Similar to **4** and **5**, the emission band is blue-shifted in relation to the corresponding unsubstituted complex **3**, supporting MLCT character of the excited state. The striking difference between complex **6** and complexes **4** and **5** concerning lack of higher energy band of singlet origin and ILCT character in the case of **6** can be explained by the smaller energy gap and faster non-radiative decay for **6** in comparison with **4** and **5**.

In more polar acetonitrile, the emission spectra of **4–6** displayed only a long-wavelength band, with a maximum at 702 nm for **4**, 741 nm for **5** and 781 nm for **6**. Compared to the parent complexes without electron-rich pyrrolidine group **1–3**, the emission maximum of **4–6** is bathochromically shifted. This behaviour is inconsistent with that expected for pure MLCT emitters. In this case the nature of the excited state seems to be ILCT. For both series **1–3** and **4–6**, bathochromic shift of the emission band was in the order pyridine < thiazole < pyrazine, consistent with the increase of π-acceptor capability (Table S9).

Upon cooling to low temperature (at 77 K in EtOH–MeOH (4:1 v/v) glassy medium), the emission of the complexes occurred at higher energy (543–632 nm), which is attributed to the rigidochromic effect. This effect is responsible for raising the energy of the emissive MLLCT states due to the lack of solvent reorganization following excitation.[26] The emission bands of **1–6** are structureless, which is consistent with the charge transfer character (Fig. S19 in supporting information). On the other hand, the microsecond excited state lifetimes in concert with large Stokes shifts are supportive of the phosphorescence assignment.

Except for **5** showing emission in two regions (Fig. S21), the solid-state emission spectra of the Re(I) complexes exhibited a single structureless band with a maximum located in the orange-red spectral region. Distinct differences in lifetimes were observed between **1–3** and **4–6**. The complexes bearing triimine ligand functionalized with pyrrolidine substituent exhibit significantly slower decay rate. For all the complexes, lifetimes fall into microsecond or sub-microsecond range and quantum yields, except for **3**, are higher than those in solution.

The Re(I) complexes, likewise the ligands, were also photoluminescent in the form of a thin film. In this case, the effect of λ_{ex} not only on PL intensity, but also on λ_{em}, is pronounced (cf. Fig. S17b). PL of all the films was dependent on excitation wavelength. Together with a decrease of λ_{ex} energy from 310 nm (4 eV) to 340 nm (3.6 eV), a bathochromic shift of λ_{em} from 375 to 413 nm was seen. In the PL spectra of complexes **1–4**, recorded using the same $\lambda_{ex,}$ two emission bands with λ_{em} at 370–380 and 572–609 nm can be distinguished. The emission spectra of all the films and blends are very similar and they are dominated by the band with λ_{em} around 380–410 nm.

In addition, λ_{em} of the complexes in the form of film was hypsochromically shifted with respect to that of the complexes in solution. This not so typical phenomenon, that is, the blue shift of the solid-state PL emission in comparison to solution, was also reported for other compounds.[27] The effect of luminophore content in matrix on PL was evaluated for compounds bearing dtpy (L^5 and **5**) (cf. Fig. 7). The shift of the peak emission to longer wavelengths with increasing doping concentration of L^5 from 1 and 2 to 15 wt% was noted, probably due to aggregation of compound with increasing content.

A higher PL quantum yield was found for the blend with 1 wt% of L^5. In the case of complex **5**, the increase of its content from 1 to 2 to 15 wt% resulted in the appearance of the second emission band at 598 nm. Blend with 2 wt% of **5** showed higher PL quantum yield with respect to matrix containing lower concentration of **5** (cf. Table S8).

2.7 | Identification of Excited Triplet State using Laser Flash Photolysis

To confirm the triplet excited state, compound **4** was studied by recording the nanosecond time-resolved transient absorption spectra in acetonitrile and chloroform, and the results are shown in Fig. 8. The positive band, spanning from *ca* 480 to *ca* 700 nm, is separated from the ground-state bleaching with well-defined isosbestic points, and the bleaching recovery is synchronous with the positive absorption decay. This indicates that the ground state is repopulated ($T_1 \rightarrow S_0$) as the positive T_1–T_n absorption decays. The decay of T_1 absorption is mono-exponential, and transient triplet state is transformed to S_0 within a submicrosecond scale. The triplet lifetime of **4** (774 ns) in argon-saturated acetonitrile is sufficiently long for photosensitizing the production of singlet oxygen ($T_1 + {}^3O_2 \rightarrow S_0 + {}^1O_2$). In air-saturated solution, there is a significant decrease of the τ_T value to 162 ns. To determine the singlet oxygen quantum yields (Φ_Δ) of **4**, the luminescence method was used.

2.8 | Electroluminescence

The EL abilities of both the ligands and complexes were investigated in diodes with guest–host configuration. As active layers in the devices, the layers of the same composition as those used for the PL measurements, that is, neat compounds and blends with PVK:PBD, were applied. Operation of a diode with a guest–host

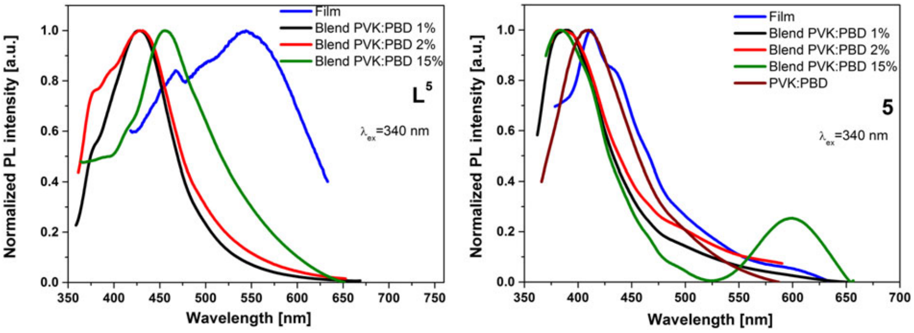

FIGURE 7 PL spectra of ligand L^5 and complex **5** in film form and blends with various compound contents.

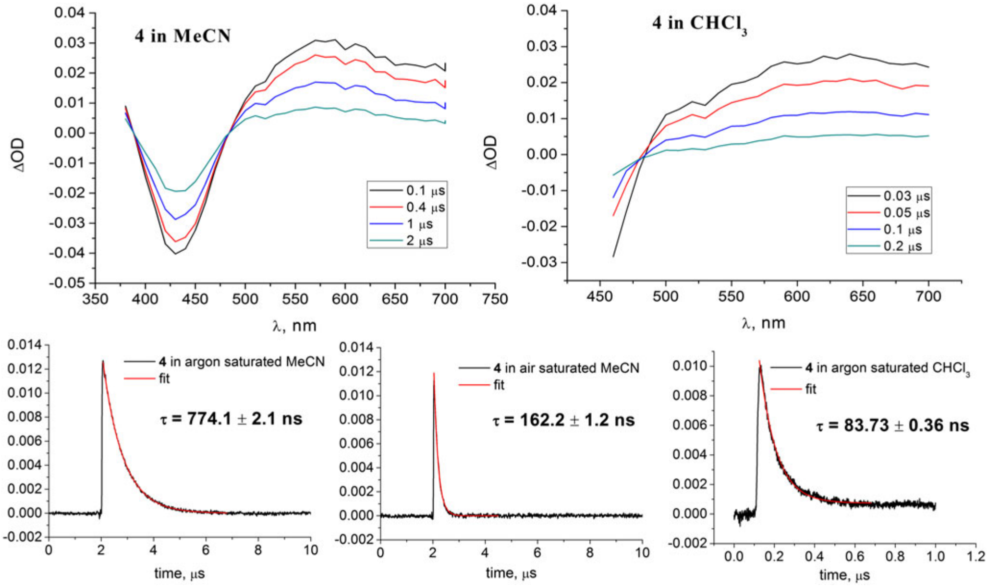

FIGURE 8 Nanosecond transient absorption spectra of **4** measured in MeCN and $CHCl_3$ at room temperature (excitation wavelength λ_{ex} of 355 nm). Transient decays were monitored at 570 nm for **4** in MeCN and at 600 nm for **4** in MeCN.

configuration is based on two mechanisms, that is, energy transfer and charge trapping.[28] In the energy transfer mechanism, singlet excitons are formed in the host matrix due to electrical excitation and they can then be transferred to the guest molecule via Förster resonance energy transfer (FRET). FRET efficiency significantly depends on the spectral overlap between the matrix emission and the luminophore absorption. In the charge trapping mechanism, the excitons are formed directly on the luminophore without the necessity of energy transfer from host to guest. For effective charge trapping, the HOMO and LUMO of the guest need to lie within the

TABLE 1 Position of λ_{EL} of light emitted by diodes and turn-on voltage together with the thickness of selected active layers

	ITO/PEDOT:PSS/compound/Al		ITO/PEDOT:PSS/PVK:PBD:compound/Al	
Code	V_{on} (V)	λ_{EL} (nm) (*d*, nm)	V_{on} (V)	λ_{EL} (nm) (*d*, nm)
L^1	1.6	—	3.4	614
L^2	1.1	— (76)	1.7	590
L^3	1.5	—	2.8	533, 580 (90)
L^4	1.5	659	1.8	590 (125)
L^5	2.6	654	2.5 2.0[a] 5.4[b]	500 473[a] 547[b] (72)
L^6	1.4	—	2.5	545
1	1.2	—	2.8	600
2	1.1	651	2.8	625
3	2.2	660	2.8	600
4	2.8	638	2.1	583
5	2.0	657	1.7 2.0[a] 6.8[b]	606 (109) 602[a] 623[b] (106)
6	1.1	655	1.0	609

[a] 1 wt% content of compound in PVK:PBD matrix.

[b] 15 wt% content of compound in PVK:PBD matrix.

bandgap of the host. Considering the UV–visible spectra of ligands, partial spectral overlap between guest absorption and PVK:PBD emission only in the case of L^4–$L^{\mathbf{6}}$ was seen (cf. Figs S12 and S14). The Re(I) complexes exhibited better spectral overlap. Based on IP and EA values, estimated from cyclic voltammetry measurements (corresponding the HOMO and LUMO energies, respectively), it can be noted that all of the compounds (except for L^1 and $L^{\mathbf{2}}$) have their HOMO and LUMO levels appropriately aligned with respect to the corresponding levels of PVK and PBD, to ensure trapping electrons from PBD and holes from PVK (cf. Fig. S17c).

Diodes with the structures ITO/PEDOT:PSS/compound/Al and ITO/PEDOT:PSS/PVK:PBD:compound/Al were fabricated. For the prepared devices, current density–voltage (*J*–*V*) characteristics were recorded up to 5 V, and for selected active layers, thickness was measured by atomic force microscopy. The obtained turn-on voltage (V_{on}), position of EL band maximum (λ_{EL}) and thickness of active layer (d) are summarized in Table 1. The representative *J*–*V* characteristics and EL spectra of diodes based on L^5 and complexes with pyrrolidine unit (**4**–**6**) together with intensity dependencies on the applied external voltage are depicted in Fig. 9. EL spectra of other diodes are presented in Fig. S20.

The turn on-voltages of all the diodes were found to be in a similar range of 1.0–2.8 V, except for device with L^1 blend, L^5 (15 wt% in matrix) and **5** (1 and 15 wt% in PVK:PBD), which were equal to 3.4, 5.4 and 4.6 and 6.8 V, respectively. Most of the fabricated diodes emitted light under external voltage differing in intensity and position of λ_{EL}, depending on both the chemical structure of the compound and the composition of the active layer. Diodes based on neat ligands without pyrrolidine

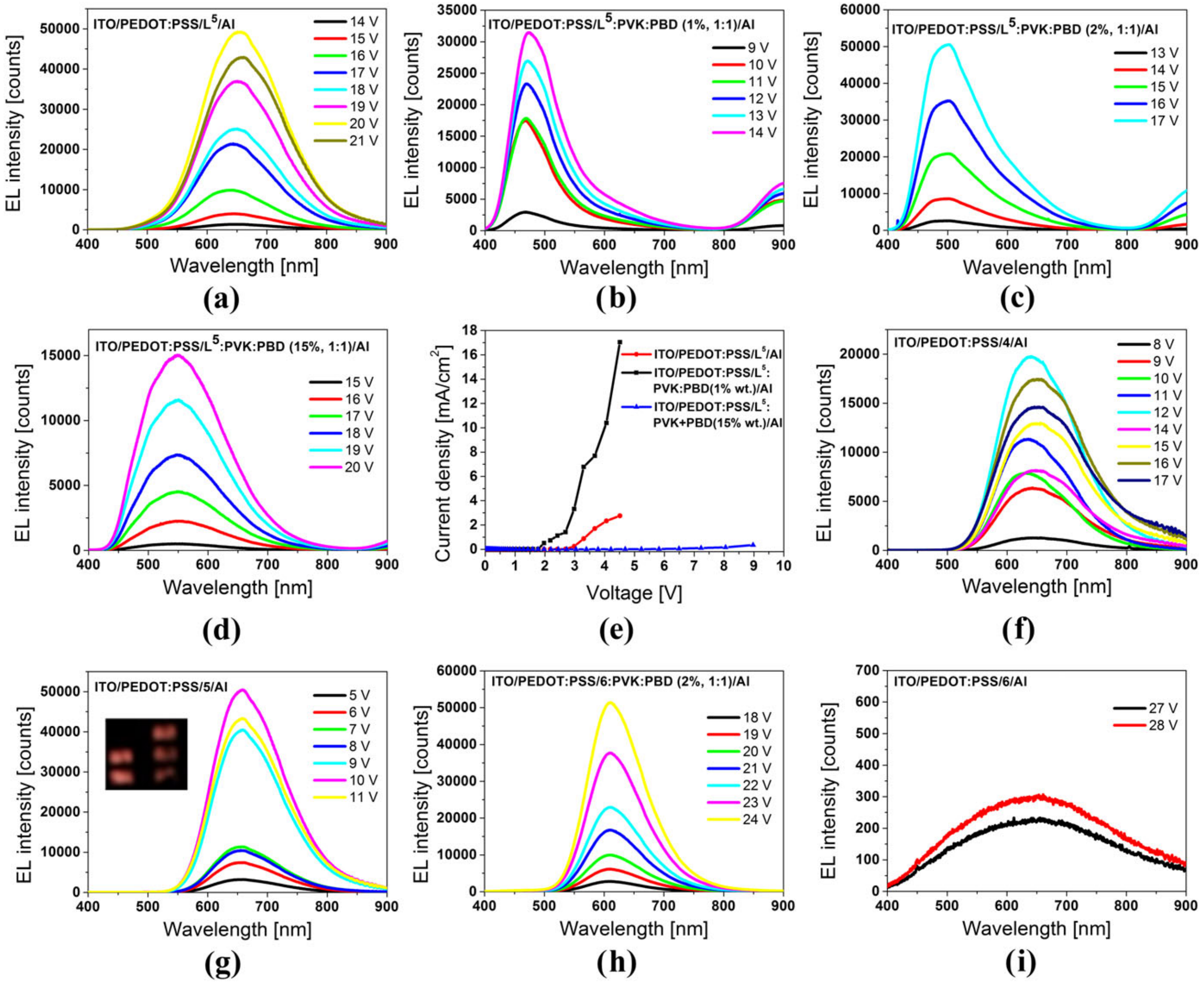

FIGURE 9 EL spectra of diodes based on (a–d) L^5 with various ligand contents in active layer together with (e) *J*–*V* characteristics and (f–i) neat complexes **4**, **5** and **6** together with device with **6** dispersed in PVK:PBD matrix.

substituent (L^1–L^3) and with dppy (L^6) did not show EL response. Other ligand-containing diodes emitted light with λ_{EL} ranging from 500 to 659 nm. The highest intensity of emitted light was found for the device containing as active layer the neat ligand with pyrrolidine and dtpy units (L^5). Considering the devices based on ligands molecularly dispersed in a matrix, it was found that the lowest EL intensity was observed in diodes with ligand bearing terpy (L^1). Increase of the ligand (L^5) content in blend resulted in bathochromic shift of λ_{EL} from blue to green spectral range. The position of λ_{EL} of light emitted by diodes containing the neat ligands and complexes was hypsochromically shifted with respect to devices with the compounds blended with PVK:PBD. Focusing on the diodes based on Re(I) complexes, it was found that only in the case of the device with the compound containing terpy without pyrrolidine unit (**1**) was no light emission observed. Utilization of the complexes blended with PVK:PBD as active layers resulted in an increase of emitted light intensity. Similar to the diode with L^5, a higher content of the complex **5** in blend shifted the λ_{EL} position to lower energy, but to a smaller extent. Considering the intensity of emitted light from diodes differing in L^5 and **5** content, it can be noted that the optimal amount of compound in blend is 2 wt%, which gives the highest intensity. All devices based on complexes emitted red light, except for **4** dispersed in a matrix (cf. Table 1). Replacement of free ligand L^4 with analogous complex **4** resulted in a slight shift of λ_{EL} from 659 to 638 nm. Generally, application as active layer of both ligands and complexes in a matrix caused an increase of emitted light intensity.

2.9 | Theoretical Calculations

DFT and time-dependent DFT (TD-DFT) methods were applied to describe the electronic structure of excited states of ligands L^1–L$^{\mathbf{6}}$ and complexes **1–6**. The excitation

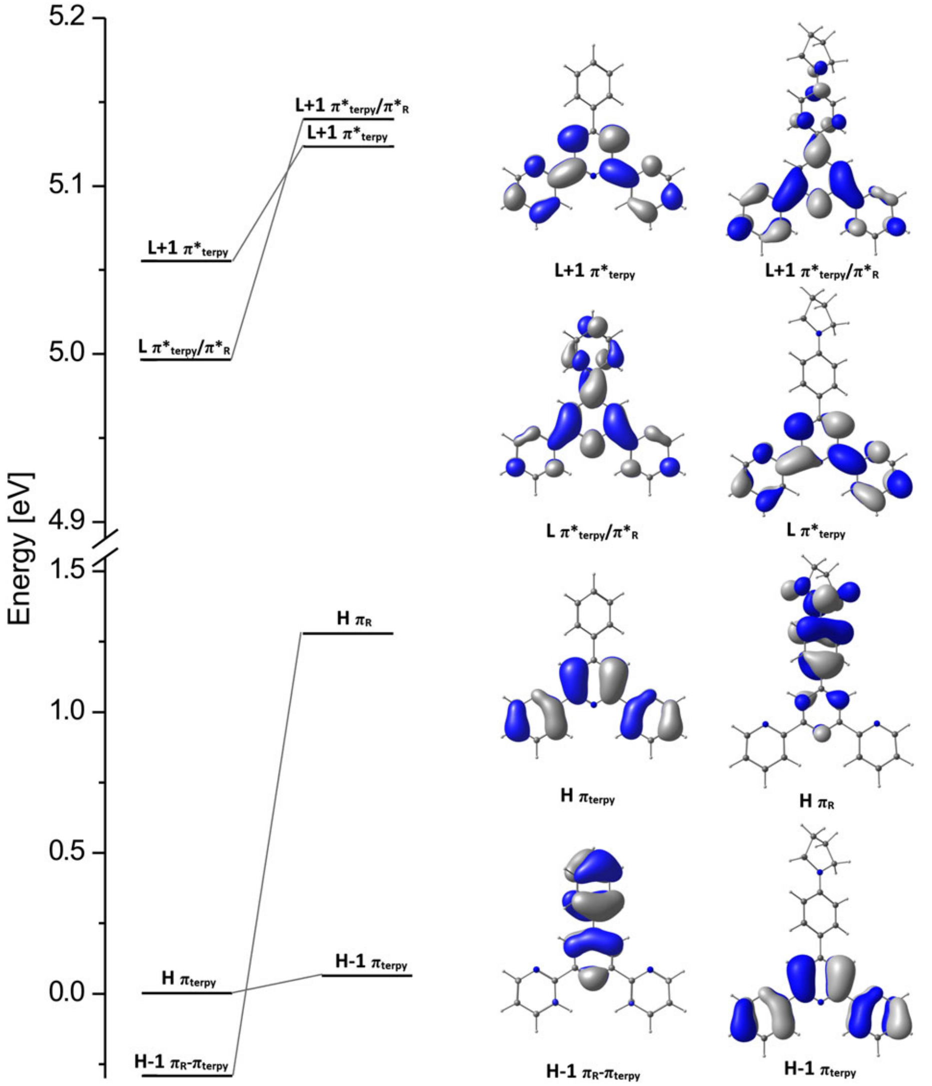

FIGURE 10 Energy diagram of frontier molecular orbitals for L^1 and L^4 ligands.

energies were calculated in the wavelength range from *ca* 200 to *ca* 500 nm. Obtained wavelengths, oscillator strengths and experimental absorption spectra are presented in Fig. 10 and Figs S22 and S23. The energies and characteristics of selected singlet electronic transitions, together with assignment to the experimental absorption bands are presented in Tables S11–S22. For L^1–$L^{\mathbf{6}}$, the electronic excitations with the largest oscillator strengths come mainly from $\pi \rightarrow \pi^*$ transitions and generally can be characterized as $\pi_L \rightarrow \pi^*_L$, $\pi_R \rightarrow \pi^*_R$ and $\pi_L/\pi_R \rightarrow \pi^*_L/\pi^*_R$ excitations, where L and R denote triimine skeleton and substituent group, respectively. In the low-energy part of the calculated spectrum, most of the mentioned electronic transitions have rather charge transfer character. Occupied and unoccupied π orbitals, involved in charge transfer electronic transitions, are localized on various parts of the molecule, namely on terpyridine/dithiazolylpyridine/dipyrazinylpyridine moiety or R substituent (Fig. 10).

Analysing the results of calculations, it is possible to notice that the energy order of the lowest excited states of $\pi_R \rightarrow \pi^*_L$, $\pi_L \rightarrow \pi^*_R$ and $\pi_L \rightarrow \pi^*_L$ type is different for L^1–L^3 and L^4–L^6 groups of ligands. For L^1 the lowest electronic transition to S_1 state with medium oscillator strength (0.2131) has $\pi_{terpy} \rightarrow \pi^*_{terpy}$ character. The next S_4, S_5 and S_6 electronic transitions of larger oscillator strength (0.3599, 0.1751, 0.3754) can be characterized in sequence as $\pi_{terpy} \rightarrow \pi^*_{terpy}/\pi^*_R$, $\pi_{terpy}/\pi_R \rightarrow \pi^*_{terpy}/\pi^*_R$ and $\pi_{terpy}/\pi_R \rightarrow \pi^*$ excitations. For L^4 the first S_1 electronic transition has very small oscillator strength (0.0002) and is of $\pi_R \rightarrow \pi^*_{terpy}/\pi^*_R$ type, while the second S_2 transition of $\pi_R \rightarrow \pi^*_{terpy}$ character has large value of oscillator strength (0.5734). Similar $\pi_R \rightarrow \pi^*_{terpy}$ character of excitation can be also assigned to S_3 electronic state. The charge transfer $\pi_{terpy} \rightarrow \pi^*_{terpy}/\pi^*_R$ and local πterpy-π^*_{terpy} transitions correspond to S^4 and S^8 excited states, for which the energy of excitation is very close to the excitation energy of similar electronic transitions for L^1. Overall, for L^1 the lowest intense electronic transition occurs to the S^1 state and it is related to the partial charge transfer from terpyridine to phenyl ring, whereas for L^4 the first intense transition involves S^2 excited state and it is an electronic excitation with the charge transfer in the opposite direction, namely from phenyl ring on terpyridine fragment.

The computational results show that the electronic structure and remaining properties of lowest excited state of the L^2, L^3 and L^5, L^6 species are very similar to those of L^1 and L^4, respectively. It can be concluded that differences in lowest excited electronic states between L^1–L^3 and L^4–L^6 are related to changes in the electronic structure resulting from the presence of pyrrolidine substituent attached to the phenyl group.

For all the ligands with electron-donor pyrrolidine substituent (L^4–L^6), in the range from about 370 to about 390 nm, calculated electronic spectra have characteristic low-lying $\pi_R \rightarrow \pi^*_L/\pi^*_R$ transition with large oscillator strength. This intense electronic excitation can be assigned to the first band in experimental spectrum. However, as can be seen in Fig. S22, it is clearly shifted in the direction of lower energies in relation to the maximum of the experimental band and the average difference between the calculated excitation energy and maximum band is about 0.36, 0.18 and 0.22 eV for L^4, L^5 and L^6, respectively. It is widely held that charge transfer excitation energies are often significantly underestimated using standard local xc-functionals. For L^4 and S_2 low-lying excited states, test calculations were performed with the use generalized gradient approximation (GGA), hybrid exchange correlation, and long-range separated exchange correlation functionals. The test calculations were performed in order to estimate the effect of the functional on the excitation energy of S_2 electronic state. Obtained results are presented in Fig. S24. Pure GGA functionals significantly underestimate the excitation energy of S_2 state. The average difference in energy between the lowest experimental band and the calculated S_2 transitions in the case of GGA functionals is equal to 1.18 eV. Hybrid functionals also underestimate energy of this excitation, but with smaller average difference, which amounts to 0.50 eV. Amongst tested hybrid functionals, two of them, M062x and BHandHLYP, are exceptions, because both overestimate the excitation energy by about 0.25 and 0.38 eV, respectively. Long-range separated functionals also overestimate or underestimate excitation energy of S_2 state. In the case of most of the tested long-range separated functionals, excitation energy to S_2 state is overestimated, by an average of around 0.55 eV; however, the two functionals OHSE1PBE and OHSE2PBE give lower excitation energies as compared to the energy of maximum of the lowest experimental band. Based on the obtained results, it is possible to suggest that most of the used hybrid exchange correlation functionals give a good approximation of the excitation energy for the S_2 electronic state.

The differences in the electronic structure of lowest excited states between L^1–L^3 and L^4–L^6 are visible very well in the molecular orbital picture (Fig. 10). The HOMO (H) in L^1 is mainly localized on terpyridine fragment; simultaneously, the occupied H − 1 orbital is localized on phenyl ring and partly on the central ring of terpyridine. In L^4, two HOMOs (H and H − 1) have very similar character, but their energy order is reversed. The lowest unoccupied orbitals, L and L + 1, in L^1 are π* antibonding orbitals. The first of them (L) is a π* orbital partially delocalized on the entire structure; the second is localized solely on terpyridine fragment. For L^4 two LUMOs have the same character, but the reversed order. The L and L + 1 are π^*_{terpy} and π^*_{terpy}/π^*_{R} orbitals, respectively. The HOMO orbital in L^4 has π_{Ph}–p_N character and is antibonding combination of π orbital of phenyl ring with p_N orbital of nitrogen in pyrrolidine substituent. This antibonding combination effectively increases the energy of the HOMO orbital compared to the similar H − 1 orbital in L^1, causing the lowest electronic excitations to be dominated by transitions of $\pi_R \rightarrow \pi^*_{terpy}$ type.

To verify the charge transfer problem of low-lying excited states of L^1 and L^4 ligands, the Λ parameter was calculated. Parameter Λ is a simple diagnostic test based on orbital overlap and may be used to help judge the reliability of excitation energies in TD-DFT.[29] It was clearly demonstrated that parameter Λ correlates with error in excitation energies, i.e. excitation energies are significantly underestimated when Λ is very small, whereas the errors tend to be smaller when Λ is large. It has also been observed that for hybrid functional and $\Lambda > 0.3$, the estimated excitation energies for charge transfer transitions have rather acceptable values. The calculated Λ parameters for ten lowest singlet excited states of L^1 and L^4 ligands are in the range from 0.2 to 0.8 (Table S23). For all $\pi \rightarrow \pi^*$ transitions with large or medium oscillator strength, Λ parameters are greater than 0.3. Only in the case of L^4 ligand, S_1, S_3 and S_9 electronic excitations with small values of oscillator strength have Λ below 0.3. These parameters are 0.27, 0.21 and 0.2 for S_1, S_3 and S_9 transitions, respectively. It should be emphasized that problematic S_2 transition for L^4 has an acceptable Λ value for the applied functional and obtained excitation energy probably should not be considerably underestimated. In summary, the charge transfer problem rather is not appreciable in the theoretical description of low-lying singlet electronic states of the investigated ligands.

The CASSCF/MS-CASPT2 level of theory was applied for additional verification of the TD-DFT results. Multistate version of CASSCF and CASPT2 was used to determine the excitation energy and the description of the electronic structure of the four lowest $\pi \rightarrow \pi^*$ excited states for L^1 and L^4. The calculations were done based on the CAS(12,12) active space. Active space contains 12 electrons as well as 6 occupied and 6 unoccupied π orbitals (Figs S25 and S26). The active space was selected to contain π orbitals, similar to those that are involved in the TD-DFT excitations, and in this way, calculated excited states should correspond to the lowest $\pi \rightarrow \pi^*$ excited states at TD-DFT level of theory. The MS-CASPT2 results, collected in Tables S17 and S18, correlate well with the TD-DFT calculations, but some differences are also apparent. For L^1 the electronic structure of S_1 and S_2 states can be characterized as $\pi_{terpy}/\pi_R \rightarrow \pi^*_{terpy}/\pi^*_R$ and $\pi_{terpy}/\pi_R \rightarrow \pi^*_{terpy}$ electronic excitations and well correspond to S_1 and S_2 states at TD-DFT level of theory. Both states come from excitations between orbitals localized mainly on the terpyridine fragment, but due to the fact that the unoccupied orbital in active space is partially delocalized on the phenyl ring (82 L, Fig. S25), some contribution of the $\pi_{terpy} \rightarrow \pi^*_R$ charge transfer excitation is also visible. The S_1 and S_2 electronic states for L^4 have $\pi_R/\pi_{terpy} \rightarrow \pi^*_{terpy}/\pi^*_R$ and $\pi_R/\pi_{terpy} \rightarrow \pi^*_{terpy}$ character and can be assigned to the first two excitations in TD-DFT calculations. Occupied orbital involved in excitation to the S_1 and S_2 state is mainly localized on the phenyl ring (98 H − 2, Fig. S26), so in contrast to the two lowest transitions for L^1, low lying electronic states for L^4 are rather associated with the dominating participation of charge transfer between R fragment and terpyridine. Excitation to S_2 state, which corresponds to a large oscillator strength (0.70), is practically a clean charge transfer transition of a $\pi_R \rightarrow \pi^*_{terpy}$ type, which remains in satisfactory accordance with TD-DFT results. The S_1 state has a more mixed character and electronic excitation for this state has a much lower value of the oscillator strength (0.02). The characteristic difference of the oscillator strength between S_1 and S_2 is very similar to that which can be observed in the TD-DFT calculations. The MS-CASPT2 results once again show the essential difference between characters of the lowest charge transfer states for ligands with the substituted and unsubstituted phenyl ring. For L^1 ligand, in which the phenyl ring is unsubstituted, intense low-lying $\pi \rightarrow \pi^*$ electronic transitions occur mainly within terpyridine motif but with some participation of terpyridine → R charge transfer transition, while in the case of substituted ring as in L^4, low-lying transition is an electron excitation mainly of a R → terpyridine charge transfer character. From an energetics point of view, the calculated MS-CASPT2 excitation energies of the two lowest transitions for L^1 and L^4 ligands are always higher in relation to appropriate values for TD-DFT states. Average difference of the calculated excitation energies, between the relation to appropriate values for TD-DFT and MS-CASPT2 results, is about 0.51 eV. Compared to the energy of maximum of the lowest experimental band, MS-CASPT2 excitation energies are also higher in energy with the exception of S_1 excitation for L^4. The calculated MS-CASPT2 S_1 and S_2 excitations energies for L^1 and L^4, respectively, are higher in energy by about 0.56 and 0.22 eV compared to the position of lowest experimental band. Lastly, it is crucial to point out that the S_2 electronic state, described as 'problematic' in the TD-DFT calculation, is also a second lowest excited state at the MS-CASPT2 level and has explicitly the $\pi_R \rightarrow \pi^*_{terpy}$ charge transfer character. Based on this result, it is possible to suggest that for L^4,

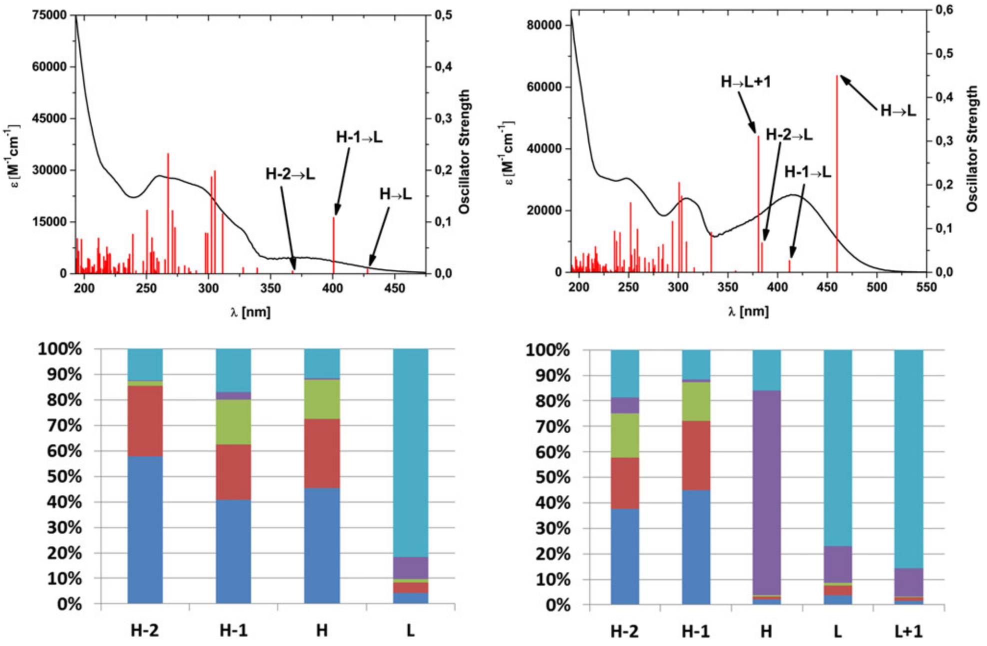

FIGURE 11 Experimental and theoretical UV–visible spectra of complexes **1** and **4** in MeCN as well as composition of selected frontier molecular orbitals (light blue, terpy; violet, R; green, Cl; red, 3CO; dark blue, Re).

excitation energy of intense S_2 transition estimated using PBE1PBE or other hybrid exchange correlation functionals well correlates with the lowest experimental band. In the case of both ligands L^1 and L^4, the remaining two electronic states (S_3 and S_4) at MS-CASPT2 level have a more complex electronic structure, and assigning them to the relevant $\pi \rightarrow \pi^*$ states at the TD-DFT level of theory becomes ambiguous and difficult.

It can be supposed that for Re(I) complexes with the ligand containing pyrrolidine substituent attached to the phenyl group, the first low-lying electronic excitation will not engage the orbitals localized on the metal, but it will be determined by the electronic transition localized only on the ligand (Fig. S27). DFT and TD-DFT studies showed that the HOMO, HOMO − 1 and HOMO − 2 orbitals of **1–3** contain significant 5d rhenium character (45, 42 and 56%, respectively) along with *ca* 25% contributions from CO component, whereas HOMOs of **4–6** are π orbitals of the trimine ligand, predominately centred on the R substituent – 80.19% for **4**, 81.42% for **5** and 80.66% for **6**. For **4–6**, the orbitals $5d_{\pi}$(Re) and π^*(CO) contribute to HOMO − 1 and HOMO − 2 and HOMO − 3. For all of **1–6**, however, the LUMOs have similar distribution and they are largely participated by π^* orbitals localized on the terpy in **1** and **4**, dtpy in **2** and **5** and dippy in **3** and **6**. The high-wavelength range of theoretical absorption spectra of **4–6** is dominated by intense transitions, mainly of ILCT ($\pi_R \rightarrow \pi^*_L$) character. This intense electronic excitation can be assigned to first band in experimental spectrum. Similar to the free ligands L^4–L^6, it is clearly shifted in the direction of lower energy in relation to the maximum of first experimental band. The difference between the calculated excitation energy and maximum band is 0.29 eV for **4**, 0.20 eV for **5** and 0.33 eV for **6**. For **1–3**, the high-wavelength range of theoretical absorption spectra comprises electronic transitions with smaller oscillator strengths (0.0034–0.1094) of MLLCT character ($d_{Re} \rightarrow \pi^*_L/\pi_{CO} \rightarrow \pi^*_L/p_{Cl} \rightarrow \pi^*_L$) and energy falling within the first experimental band (Fig. 11).

The energies of phosphorescence emissions for **1–6** were calculated from the optimization of the first triplet excited state and from the energy difference between the ground singlet and the triplet state $\Delta E_{T_1-S_0}$. As shown in Table S26, the lowest lying triplet state of Re(I) complexes **1–3** has mainly ^{3}MLLCT character, while ^{3}ILCT character dominates in T_1 for remaining complexes with the triimine ligand decorated with the pyrrolidine substituent (**4–6**).

3 | CONCLUSIONS

To summarize, a series of triimine ligands, varied in the chemical structure of peripheral rings (pyridine, thiazole and pyrazine) and the presence or absence of pyrrolidine substituent, as well as their corresponding Re(I) carbonyls were prepared and investigated. The spectral and electrochemical properties of the ligands and Re(I) complexes bearing electron-rich pyrrolidine group were strongly influenced by ILCT transitions. For compounds **4–6**, different emission profiles were found in polar and non-polar solvents, indicating change in the character of the excited state. In chloroform, presence of two emitting states, identified as an ^{1}ILCT excited state deactivated at higher energies and a longer-lived red-shifted phosphorescence attributed to the ^{3}MLCT excited state, was evidenced in the case of **4** and **5**. On the contrary, the emission of **4–6** in acetonitrile, bathochromically shifted compared to that for the corresponding **1–3**, seems to be of ILCT nature. Consistent with increase of π-acceptor capability in the order pyridine < thiazole < pyrazine, the emission of the free ligand and Re(I) complexes bearing dppy unit was significantly red-shifted in relation to the corresponding analogues incorporating terpy moiety.

All of the synthesized compounds showed high melting points ranging from 201 to 349°C, higher in the case of Re(I) complexes. The beginning of decomposition was noted above T_m and Re(I) complexes showed higher T_5 (221–354°C) value than the corresponding ligands. All the ligands with pyrrolidine substituent and complex bearing dtpy (**5**) exhibited behaviour of molecular glasses with T_g from 74 to 93 and 205°C. The presence of dppy unit in the ligand and complex increases both T_m and T_g values, but slightly reduced their solubility. The lack of pyrrolidine substituent attached to the phenyl group lowers their solubility. The Re(I) complexes showed a lower EA value, about 0.61–0.84 eV, than the analogous ligands. Pyrrolidine moiety in the ligands increases the IP value. Diodes with active layer consisting of neat ligands and complex **1** did not show an EL response contrary to others. However, in most cases, better device performance was found in diodes with guest–host configuration. Generally, diodes based on ligands emitted green light with λ_{EL} located between 500 and 590 nm. In all devices with complexes (except for **4**), red emission with λ_{EL} in the range 600–657 nm was seen. Considering the results of the preliminary EL investigations, it can be pointed out that the most promising for further OLED parameter estimation, including also modification of diode architecture, seems to be the compounds bearing pyrrolidine substituent, that is, ligands without terpy (L^5 and L^6) and the corresponding complexes (**4–6**).

4 | EXPERIMENTAL

4.1 | Materials

Re(CO)$_5$Cl (Sigma Aldrich), poly(9-vinylcarbazole) (PVK; M_n = 25 000–50 000 g mol^{-1}; Sigma Aldrich), poly(3,4(ethylenedioxy)thiophene):polystyrenesulfonate (PEDOT:PSS; 0.1–1.0 S cm^{-1}) and substrates with pixilated ITO anodes (supplied by Ossila) as well as all solvents for synthesis (of reagent grade) and for spectroscopic studies (of HPLC grade) were commercially available and they were used without further purification. The films and blends with PVK:PBD (50:50 w/w) on a glass substrate as well as all the devices with configurations ITO:PEDOT:PSS/compound/Al and ITO:PEDOT:PSS/PVK:PBD:compound/Al with complex content of 15, 2 and 1 wt% in blend were prepared according to the method reported in our previous work.[11]

4.2 | General Synthesis Route of Ligands (L^1–L^6)

Ketone (20 mmol; 2-acetylpyridine, 2-acetylthiazole or 2-acetylpyrazine) was added to a solution of aldehyde (10 mmol; benzaldehyde or 4-pyrrolidinobenzaldehyde) in ethanol (75 ml). KOH (1.54 g, 27.5 mmol) and aqueous NH_3 (35 ml) were then added. The solution was stirred at room temperature for 24 h. The solid was collected by filtration and washed with water. Recrystallization from ethanol (L^1 and L^4) or toluene (L^2, L^3, L^5 and L^6) afforded a crystalline solid.

L^1: Yield: 45%. ^{1}H NMR (400 MHz, CDCl$_3$, δ, ppm): 8.75 (s, 2H), 8.74–8.71 (m, 2H), 8.66 (d, J = 8.0 Hz, 2H), 7.90 (d, J = 7.1 Hz, 2H), 7.85 (dt, J = 7.7, 1.8 Hz, 2H), 7.53–7.42 (m, 3H), 7.34–7.31 (m, 2H). ^{13}C NMR (100 MHz, CDCl$_3$, δ, ppm): 156.37, 156.03, 150.41, 149.23, 138.61, 136.92, 129.10, 129.01, 127.44, 123.89, 121.44, 119.02. HRMS (ESI): calcd for $C_{21}H_{16}N_3$ [M + H]$^+$ 310.1344; found 310.1353.

L^2: Yield: 52%. ^{1}H NMR (400 MHz, CDCl$_3$, δ, ppm): 8.47 (s, 2H), 7.97 (d, J = 3.2 Hz, 2H), 7.87–7.83 (m, 2H), 7.57–7.46 (m, 5H). ^{13}C NMR (100 MHz, CDCl$_3$, δ, ppm): 168.93, 151.71, 150.96, 144.26, 137.43, 129.76, 129.27, 127.35, 122.00, 118.00. HRMS (ESI): calcd for $C_{17}H_{12}N_3S_2$ [M + H]$^+$ 322.0473; found 322.0473.

L^3: Yield: 57%. ^{1}H NMR (400 MHz, CDCl$_3$, δ, ppm): 9.87 (s, 2H), 8.73 (s, 2H), 8.68–8.65 (m, 4H), 7.90–7.84 (m, 2H), 7.58–7.45 (m, 3H). ^{13}C NMR (100 MHz, CDCl$_3$, δ, ppm): 154.65, 151.00, 144.93, 143.88, 143.86, 143.69, 129.60, 129.29, 127.39, 120.05. HRMS (ESI): calcd for $C_{19}H_{14}N_5$ [M + H]$^+$ 312.1249; found 312.1248.

L^4: Yield: 39%. ^{1}H NMR (400 MHz, CDCl$_3$, δ, ppm): 8.73 (d, J = 4.7 Hz, 2H), 8.71 (s, 2H), 8.66 (d, J = 8.4 Hz, 2H), 7.90–7.84 (m, 4H), 7.36–7.31 (m, 2H), 6.66 (d, J = 8.4 Hz, 2H), 3.37 (t, J = 5.9 Hz, 4H), 2.09–1.99 (m, 4H). ^{13}C NMR (100 MHz, CDCl$_3$, δ, ppm): 156.84, 155.72, 150.28, 149.14, 148.70, 136.89, 128.22, 124.60, 123.68, 121.48, 117.44, 111.92, 47.69, 25.59. HRMS (ESI): calcd for $C_{25}H_{23}N_4$ [M + H]$^+$ 379.1923; found 379.1924.

L^5: Yield: 43%. ^{1}H NMR (400 MHz, CDCl$_3$, δ, ppm): 8.42 (s, 2H), 7.96 (d, J = 3.2 Hz, 2H), 7.79 (d, J = 8.8 Hz, 2H), 7.47 (d, J = 3.2 Hz, 2H), 6.63 (d, J = 8.8 Hz, 2H), 3.35 (t, J = 6.5 Hz, 4H), 2.05–2.01 (m, 4H). ^{13}C NMR

(100 MHz, CDCl$_3$, δ, ppm): 169.59, 151.35, 150.75, 149.07, 144.07, 128.19, 123.23, 121.67, 116.22, 112.02, 47.70, 25.61. HRMS (ESI): calcd for $C_{21}H_{19}N_4S_2$ $[M + H]^+$ 391.1051; found 391.1053.

L^6: Yield: 54%. ^{1}H NMR (400 MHz, CDCl$_3$, δ, ppm): 9.87 (s, 2H), 8.69 (s, 2H), 8.68–8.64 (m, 4H), 7.85 (d, J = 8.8 Hz, 2H), 6.78 (d, J = 8.4 Hz, 2H), 3.42 (t, J = 6.5 Hz, 4H), 2.13–2.05 (m, 4H). ^{13}C NMR (100 MHz, CDCl$_3$, δ, ppm): 154.31, 151.51, 150.84, 149.11, 144.64, 143.91, 143.60, 128.22, 124.03, 118.40, 112.17, 47.79, 25.64. HRMS (ESI): calcd for $C_{23}H_{21}N_6$ $[M + H]^+$ 381.1828; found 381.1828.

4.3 | [ReCl(CO)$_3$(L^n-κ^{2}N)] Complexes (1–6)

Re(I) carbonyl complexes were prepared using Re(CO)$_5$Cl (0.10 g, 0.27 mmol) and appropriate ligand L^n (0.27 mmol) according to the procedure given in our previous paper.[11]

1: Yield: 75%. IR (KBr, cm^{-1}): 2018(vs), 1916(vs) and 1876(vs) ν(C≡O); 1614(m), 1583(w) and 1539(w) ν(C=N) and ν(C=C). ^{1}H NMR (400 MHz, DMSO-d_6, δ, ppm): 9.08 (t, J = 7.3 Hz, 3H), 8.80 (d, J = 3.8 Hz, 1H), 8.38 (t, J = 7.8 Hz, 1H), 8.22–8.15 (m, 3H), 8.06 (t, J = 7.5 Hz, 1H), 7.91 (d, J = 7.7 Hz, 1H), 7.78 (t, J = 6.2 Hz, 1H), 7.65–7.60 (m, 4H). ^{13}C NMR (100 MHz, DMSO-d_6, δ, ppm): 198.22, 194.90, 191.42 (3CO), 161.91, 158.25, 157.61, 156.70, 153.17, 151.21, 149.70, 140.46, 137.43, 135.23, 131.43, 129.87, 128.31, 127.95, 125.94, 125.63, 125.45, 124.86, 121.12. HRMS (ESI): calcd for $C_{24}H_{15}ClN_3O_3Re$ $[M - Cl]^+$ 579.55 g mol^{-1}; found 580.07 g mol^{-1}.

2: Yield: 75%. IR (KBr, cm^{-1}): 2021(vs), 1913(vs) and 1887(vs) ν(C≡O); 1611(s) and 1542(w) ν(C=N) and ν(C=C). ^{1}H NMR (400 MHz, acetone-d_6, δ, ppm): 8.84 (s, 1H), 8.37 (d, J = 3.2 Hz, 1H), 8.27 (s, 2H), 8.14 (dd, J = 5.7, 2.6 Hz, 3H), 8.09 (d, J = 3.0 Hz, 1H), 7.64 (d, J = 1.1 Hz, 1H), 7.63 (d, J = 2.4 Hz, 2H). ^{13}C NMR not recorded due to insufficient complex solubility. HRMS (ESI): calcd for $C_{20}H_{11}ClN_3O_3ReS_2Na$ $[M + Na]^+$ 650.10 g mol^{-1}; found 649.93 g mol^{-1}.

3: Yield: 70%. IR (KBr, cm^{-1}): 2030(vs), 1932(s) and 1880(vs) ν(C≡O); 1615(s) ν(C=N) and ν(C=C). ^{1}H NMR (400 MHz, DMSO-d_6,:δ, ppm): 10.36 (s, 1H), 9.35 (s, 1H), 9.16 (s, 1H), 9.14 (d, J = 2.1 Hz, 1H), 8.99 (d, J = 3.0 Hz, 1H), 8.93 (s, 2H), 8.44 (s, 1H), 8.27–8.22 (m, 2H), 7.65 (d, J = 3.4 Hz, 3H).^{13}C NMR (125 MHz, DMSO-d_6, δ, ppm): 196.99, 195.05, 190.02 (3CO), 159.24, 155.98, 153.96, 151.51, 151.43, 148.39, 147.57, 146.35, 145.78, 144.58, 134.81, 131.77, 129.94, 128.47, 126.00, 122.19. HRMS (ESI): calcd for $C_{22}H_{13}ClN_5O_3Re$ $[M - Cl]^+$ 581.53 g mol^{-1}; found 582.06 g mol^{-1}.

4: Yield: 75%. IR (KBr, cm^{-1}): 2019(vs), 1912(s) and 1886(vs) ν(C≡O); 1597(s), 1526(m) ν(C=N) and ν(C=C). ^{1}H NMR (400 MHz, DMSO-d_6, δ, ppm): 9.09 (d, J = 8.2 Hz, 1H), 9.04 (d, J = 5.3 Hz, 1H), 8.94 (s, 1H), 8.78 (d, J = 4.7 Hz, 1H), 8.37 (t, J = 7.9 Hz, 1H), 8.12 (d, J = 8.8 Hz, 2H), 8.04 (d, J = 9.5 Hz, 2H), 7.86 (d, J = 7.8 Hz, 1H), 7.78–7.73 (m, 1H), 7.61 (dd, J = 7.4, 4.9 Hz, 1H), 6.71 (d, J = 8.8 Hz, 2H), 3.38 (t, J = 5.6 Hz, 4H), 2.01 (t, J = 6.3 Hz, 4H).^{13}C NMR (100 MHz, DMSO-d_6, δ, ppm): 198.33, 195.03, 191.65 (3CO), 161.55, 158.58, 157.19, 157.02, 153.30, 153.07, 150.67, 149.64, 140.32, 137.32, 129.38, 127.69, 125.68, 125.54, 125.25, 122.59, 119.11, 114.94, 48.48, 25.39, 24.40. HRMS (ESI): calcd for $C_{28}H_{22}ClN_4O_3ReNa$ $[M + Na]^+$ 707.14 g mol $^{-1}$; found 707.08 g mol^{-1}.

5: Yield: 80%. IR (KBr, cm^{-1}): 2019(vs), 1912(s) and 1886(vs) ν(C≡O); 1589(s), 1534(m) ν(C=N) and ν(C=C). ^{1}H NMR (400 MHz, acetone-d_6, δ, ppm): 8.67 (s, 1H), 8.33 (d, J = 3.3 Hz, 1H), 8.21 (d, J = 3.3 Hz, 1H), 8.12 (s, 2H), 8.06 (s, 1H), 8.04 (d, J = 2.7 Hz, 2H), 6.75 (d, J = 8.8 Hz, 2H), 3.43 (t, J = 6.5 Hz, 4H), 2.10 (s, 4H).^{13}C NMR not recorded due to insufficient complex solubility. HRMS (ESI): calcd for $C_{24}H_{18}ClN_4O_3S_2ReNa$ $[M + Na]^+$ 719.18 g mol^{-1}; found 719.0 g mol^{-1}.

6: Yield: 70%. IR (KBr, cm^{-1}): 2023(vs), 1932(s) and 1890(vs) ν(C≡O); 1594(s), 1535(m) ν(C=N) and ν(C=C). ^{1}H NMR (400 MHz, DMSO-d_6, δ, ppm): 10.34 (s, 1H), 9.17 (d, J = 1.8 Hz, 1H), 9.11 (d, J = 1.2 Hz, 2H), 8.96 (d, J = 3.0 Hz, 1H), 8.90 (t, J = 2.2 Hz, 2H), 8.25 (d, J = 1.8 Hz, 1H), 8.18 (d, J = 9.0 Hz, 2H), 6.72 (d, J = 9.0 Hz, 2H), 3.38 (d, J = 6.5 Hz, 4H), 2.01 (t, J = 6.4 Hz, 4H).13C NMR not recorded due to insufficient complex solubility. HRMS (ESI): calcd for $C_{26}H_{20}N_6O_3ReCl$ $[M + Na]^+$ 709.13 g mol^{-1}; found 709.07 g mol^{-1}.

4.4 | Crystal Structure Determination and Refinement

The X-ray diffraction data of **1–6** were collected with a Gemini A Ultra diffractometer (Mo Kα radiation; λ = 0.71073 Å) using a procedure reported previously.[11] Details of the crystallographic data collection, structural determination and refinement[30,31] for **1–6** are given in Table S4.

4.5 | Physical Measurements

Infrared (IR) spectra (KBr pellets) were measured with a Nicolet iS5 FTIR spectrophotometer (400–4000 cm^{-1}). Absorption spectral measurements were carried out using a Thermo Scientific Evolution 220 UV/Vis spectrometer (in solution) and a Jasco V570 UV–Vis–NIR spectrometer (in solid state as film deposited on a glass substrate and as blends with PVK:PBD on a glass substrate). ^{1}H NMR and

^{13}C NMR spectra were collected (295 K) with a Bruker Avance 400 NMR spectrometer or Bruker Avance 500 NMR spectrometer.

Electrospray ionization mass spectrometry (ESI-MS) was performed with a Varian 500-MS IT mass spectrometer ion trap apparatus using a procedure reported previously.[11]

Steady-state emission measurements of solid-state and solution samples were carried out with an FLS-980 fluorescence spectrophotometer. To determine the PL lifetimes, time-correlated single-photon counting or multi-channel scaling method was used. PL spectra in solid state as film deposited on a glass substrate and as blends with PVK:PBD on a glass substrate were collected with a Hitachi F-2500 spectrometer. A precise voltage supply (Gw Instek PSP-405) with the sample fixed to an XYZ stage was applied to collect EL spectra, and all the measurements were performed using a procedure reported in our previous work.[11]

Differential scanning calorimetry studies were carried out with the use of a TA-DSC 2010 apparatus under nitrogen atmosphere, with a heating rate of 20°C min^{-1}. An ATLAS 0531 electrochemical unit and impedance analyser potentiostat was used to perform electrochemical measurements.[11] Thickness of active layers was determined with atomic force microscopy (Topometrix Explorer TMX 2000).

4.6 | Computational Details

The calculations (geometry optimization, absorption and emission spectra) were performed using the Gaussian-09 program package[22] at the DFT level with the PBE1PBE hybrid exchange correlation functional, and the def2-TZVPD basis set for rhenium and def2-TZVP basis set for other elements.[32–34]

To verify the charge transfer problem at the TD-DFT level of theory, the Λ parameter[29] was calculated for ten lowest singlet excited states of L^1 and L^4 ligands. For optimized geometries of L^1 and L^4 ligands, ten lowest electronic transitions were recalculated using the Gamess program[35] and the same method described above. In calculations, ligand environment was taken into account by using the polarizable continuum model (PCM) and acetonitrile as solvent. The solvation model density[36] implemented in the Gamess package was applied for PCM electrostatics. To examine the properties of the four low-lying singlet excited states of L^1 and L^4, the CASSCF[37] and MS-CASPT2[38] level calculations were carried out with MOLCAS[39] quantum chemical package. The CASSCF/MS-CASPT2 calculations were performed using the ANO-L[40] basis set, assuming the PBE1PBE/def2-TZVPD/def2-TZVP optimized geometry of L^1 and L^4. The ANO-L basis was used with the contractions 3s2p1d for nitrogen and carbon, and 2s for hydrogen. Several active spaces were tested and finally a CAS(12,12) space was used to describe the lowest $\pi \rightarrow \pi^*$electronic excitations. The selected space contains 12 electrons and 6 occupied and 6 unoccupied π orbitals, the character of which is similar to those involved in TD-DFT transitions. PCM/acetonitrile solvation model was used to incorporate the effects of the solvent.

4.7 | Nanosecond Laser Flash Photolysis

Samples for time-resolved photolysis were excited at 355 nm (third harmonic of a Nd:YAG laser). Nd:YAG laser pulses (Spectra Physics, Mountain View, CA, USA, model INDI 40-10) of 6–8 ns duration were employed. The monitoring system consisted of a 150 W pulsed Xe lamp with a lamp pulser (Applied Photophysics, Surrey, UK), a monochromator (Princeton Instruments, Spectra Pro SP-2357, Acton, MA, USA) and an R955 photomultiplier (Hamamatsu, Japan), powered by a PS-310 power supply (Stanford Research System, Sunnyvale, CA, USA). The data processing system consisted of real-time acquisition using a digital oscilloscope (WaveRunner 6100A, LeCroy, Chestnut Ridge, NY, USA) which was triggered by a fast photodiode (Thorlabs, DET10M, *ca* 1 ns rise time) and transferred to a computer equipped with software based on LabView 8.0 (National Instruments, Austin, TX, USA) which controlled the timing and acquisition functions of the system. The experiments were carried out in rectangular 1 cm × 1 cm quartz cells at room temperature.

ACKNOWLEDGEMENTS

The research was co-financed by Narodowe Centrum Nauki grant no. DEC-2017/25/B/ST5/01611. The calculations were carried out in Wroclaw Centre for Networking and Supercomputing (http://www.wcss.wroc.pl). The authors thank Dr H. Janeczek for differential scanning calorimetry measurements.

ORCID

Barbara Machura http://orcid.org/0000-0001-7688-6491

REFERENCES

[1] a) D. J. Stufkens, A. Vlček Jr., *Coord. Chem. Rev.* **1998**, *177*, 127. b) R. A. Kirgan, B. P. Sullivan, D. P. Rillema, *Top. Curr. Chem.* **2007**, *281*, 45. c) A. Cannizzo, A. M. Blanco-Rodríguez, A. El Nahhas, J. Šebera, S. Záliš, A. Vlček Jr., M. Chergui, *J. Am. Chem. Soc.* **2008**, *130*(28), 8967. d) A. Kumar, A. S. Sun, A. J.

Lees, *Top. Organometal. Chem.* **2010**, *29*, 1. e) A. Vlček Jr., *Top. Organometal. Chem.* **2010**, *29*, 73. f) R. Baková, M. Chergui, C. Daniel, A. Vlček Jr., S. Záliš, *Coord. Chem. Rev.* **2011**, *255*, 975. gS. Záliš, C. J. Milne, A. El Nahhas, A. M. Blanco-Rodríguez, R. M. van der Veen, A. Vlček Jr., *Inorg. Chem.* **2013**, *52*(10), 5775. h)A. El Nahhas, R. M. van der Veen, T. J. Penfold, V. T. Pham, F. A. Lima, R. Abela, A. M. Blanco-Rodriguez, S. Záliš, A. Vlček, I. Tavernelli, U. Rothlisberger, C. J. Milne, M. Chergui, *J. Phys. Chem. A* **2013**, *117*(2), 361. i) C. Daniel, *Coord. Chem. Rev.* **2015**, *282–283*, 19. j) K. M.-C. Wong, C. Wang, H.-C. Lam, N. Zhu, *Polyhedron* **2015**, *86*, 133. k) A. Świtlicka-Olszewska, T. Klemens, I. Nawrot, B. Machura, R. Kruszynski, *J. Lumin.* **2016**, *171*, 166. l) A. Świtlicka, T. Klemens, B. Machura, E. Schab-Balcerzak, K. Laba, M. Lapkowski, M. Grucela, J. Nycz, M. Szala, M. Kania, *RSC Adv.* **2016**, *6*, 112908. m) S. Mai, H. Gattuso, M. Fumanal, A. Munoz-Losa, A. Monari, C. Daniel, L. González, *Phys. Chem. Chem. Phys.* **2017**, *19*, 27240. n) C.-C. Ko, V. Wing-Wah Yam, *Acc. Chem. Res.* **2018**, *51*, 149. o) D. A. Kurtz, K. R. Brereton, K. P. Ruoff, H. M. Tang, G. A. N. Felton, A. J. M. Miller, J. L. Dempsey, *Inorg. Chem.* **2018**, *57*, 5389.

[2] M. Wrighton, D. L. Morse, *J. Am. Chem. Soc.* **1974**, *96*, 998.

[3] a) T. Morimoto, J. Tanabe, K. Sakamoto, K. Koike, O. Ishitani, *Res. Chem. Intermed.* **2013**, *39*, 437. b) E. Portenkirchner, D. Apaydin, G. Aufischer, M. Havlicek, M. White, M. C. Scharber, N. Serdar Sariciftci, *ChemPhysChem* **2014**, *15*, 3634. c) A. Zarkadoulas, E. Koutsouri, C. Kefalidi, C. A. Mitsopoulou, *Coord. Chem. Rev.* **2015**, *304–305*, 55. d) J. K. Nganga, C. R. Samanamu, J. M. Tanski, C. Pacheco, C. Saucedo, V. S. Batista, K. A. Grice, M. Z. Ertem, A. M. Angeles-Boza, *Inorg. Chem.* **2017**, *56*, 3214. e) J. F. Martinez, N. T. La Porte, M. R. Wasielewski, *J. Phys. Chem. C* **2018**, *122*, 2608.

[4] a) R.-R. Ye, C.-P. Tan, M.-H. Chen, L. Hao, L.-N. Ji, Z.-W. Mao, *Chem. Eur. J.* **2016**, *22*, 7800. b) S. Hostachy, C. Policar, N. Delsuc, *Coord. Chem. Rev.* **2017**, *351*, 172. c) L. C.-C. Lee, K.-K. Leung, K. Kam-Wing Lo, *Dalton Trans.* **2017**, *46*, 16357. d) M. T. Gabr, F. C. Pigge, *Dalton Trans.* **2017**, *46*, 15040.

[5] a) C.-O. Ng, S.-W. Lai, H. Feng, S.-M. Yiu, C.-C. Ko, *Dalton Trans.* **2011**, *40*, 10020. b) K. K.-W. Lo, M.-W. Louie, K. Y. Zhang, *18th Int. Symp. Photochem. Photophys. Coord. Compd. Sapporo 2009* **2010**, *254*, 2603. c) G. Xu, M. Lu, C. Huang, Y. Wang, S. Ge, *Spectrochim. Acta. A* **2014**, *123*, 369. d) A. Ramdass, V. Sathish, E. Babu, M. Velayudham, P. Thanasekaran, S. Rajagopal, *Coord. Chem. Rev.* **2017**, *343*, 278. e) A. Ramdass, V. Sathish, M. Velayudham, P. Thanasekaran, S. Umapathy, S. Rajagopal, *Sens. Actuators B* **2017**, *240*, 1216.

[6] a) A. Fernández-Acebes, J.-M. Lehn, *Chem. Eur. J.* **1999**, *5*, 3285. b) S.-S. Sun, E. Robson, N. Dunwoody, A. S. Silva, I. M. Brinn, A. J. Lees, *Chem. Commun.* **2000**, 201. c) J. D. Lewis, R. N. Perutz, J. N. Moore, *Chem. Commun. 2000*, 1865. d) A. O. T. Patrocinio, K. P. M. Frin, N. Y. Murakami Iha, *Inorg. Chem.* **2013**, *52*, 5889. e) V. Sathish, A. Ramdass, P. Thanasekaran, K.-L. Lu, S. Rajagopal, J. Photochem, *C* **2015**, *23*, 25.

[7] a) R. C. Evans, P. Douglas, C. J. Winscom, *Coord. Chem. Rev.* **2006**, *250*, 2093. b) M. V. Werrett, G. S. Huff, S. Muzzioli, V. Fiorini, S. Zacchini, B. W. Skeleton, A. Maggiore, J. M. Malicka, M. Cocchi, K. C. Gordon, S. Stagni, M. Massi, *Dalton Trans.* **2015**, 8379. c) G.-W. Zhao, J.-H. Zhao, Y.-X. Hu, D.-Y. Zhang, X. Li, *Synth. Met.* **2016**, *212*, 131. d) Y.-X. Hu, G.-W. Zhao, Y. Dong, Y.-L. Lü, X. Li, D.-Y. Zhang, *Dyes Pigm* **2017**, *137*, 569. e) X. Li, G.-W. Zhao, Y.-X. Hu, J.-H. Zhao, Y. Dong, L. Zhou, Y.-L. Lv, H.-J. Chi, Z.-J. Su, *Mater. Chem. C* **2017**, *5*, 7629.

[8] a) A. I. Baba, J. R. Shaw, J. A. Simon, R. P. Thummel, R. H. Schmehl, *Coord. Chem. Rev.* **1998**, *171*, 43. b) M. P. Coogan, V. Fernández-Moreira, B. M. Kariuki, S. J. A. Pope, F. L. Thorp-Greenwood, *Angew. Chem. Int. Ed.* **2009**, *48*, 4965. c) A. J. Amoroso, A. Banu, M. P. Coogan, P. G. Edwards, G. Hossain, K. M. A. Malik, *Dalton Trans.* **2010**, *39*, 6993. d) F. Zhao, W. Q. Liu, H. Ying Xia, Y. Bo Wang, *Comput. Theor. Chem.* **2012**, *997*, 49. e) D. Wang, Q.-L. Xu, S. Zhang, H.-Y. Li, C.-C. Wang, T.-Y. Li, Y. M. Jing, W. Huang, Y. X. Zheng, G. Accorsi, *Dalton Trans.* **2013**, *42*, 2716. f) H. van der Salm, C. B. Larsen, J. R. W. McLay, M. G. Fraser, N. T. Lucas, K. C. Gordon, *Dalton Trans.* **2014**, *43*, 17775. g) B. Laramee-Milette, C. Lachance-Brais, G. S. Hanan, *Dalton Trans.* **2015**, *44*, 41. h) T. Klemens, A. Switlicka-Olszewska, B. Machura, M. Grucela, E. Schab-Balcerzak, K. Smolarek, A. Mackowski, A. Szlapa, S. Kula, S. Krompiec, P. Lodowski, A. Chrobok, *Dalton Trans.* **2016**, *45*, 1746. i) T. Klemens, A. Świtlicka-Olszewska, B. Machura, M. Grucela, H. Janeczek, E. Schab-Balcerzak, A. Szlapa, S. Kula, S. Krompiec, K. Smolarek, D. Kowalska, S. Mackowski, K. Erfurt, P. Lodowski, *RSC Adv.* **2016**, *6*, 56335. j) L. D. Ramos, R. N. Sampaio, F. F. de Assis, K. T. de Oliveira, P. Homem-de-Mello, A. O. T. Patrocinio, K. P. M. Frin, *Dalton Trans.* **2016**, *45*, 11688.

[9] a) Y. Yue, T. Grusenmeyer, Z. Ma, P. Zhang, T. Tat Pham, J. T. Mague, J. P. Donahue, R. H. Schmehl, D. N. Beratan, I. V. Rubtsov, *J. Phys. Chem. B* **2013**, *117*, 15903. b) Y.-X. Peng, D. Xu, N. Wang, T. Tao, B. Hua, W. Huang, *Tetrahedron* **2016**, *72*, 3443.

[10] a) C. Jia, S.-X. Liu, C. Tanner, C. Leiggener, A. Neels, L. Sanguinet, E. Levillain, S. Leutwyler, A. Hauser, S. Decurtins, *Chem. Eur. J.* **2007**, *13*, 3804. b) M. G. Fraser, A. G. Blackman, G. I. S. Irwin, C. P. Easton, K. C. Gordon, *Inorg. Chem.* **2010**, *49*, 5180. c) C. B. Larsen, H. van der Salm, C. A. Clark, A. B. S. Elliott, M. G. Fraser, R. Horvath, N. T. Lucas, X.-Z. Sun, M. W. George, K. C. Gordon, *Inorg. Chem.* **2014**, *53*, 1339. d) H. van der Salm, C. B. Larsen, J. R. W. McLay, G. S. Huff, K. C. Gordon, *Inorg. Chim. Acta* **2015**, *428*, 1. e) C. B. Larsen, H. van der Salm, G. E. Shillito, N. T. Lucas, K. C. Gordon, *Inorg. Chem.* **2016**, *55*, 8446. f) B. S. Adams, G. E. Shillito, H. van der Salm, R. Horvath, C. B. Larsen, X.-Z. Sun, N. T. Lucas, M. W. George, K. C. Gordon, *Inorg. Chem.* **2017**, *56*, 12967.

[11] a) L. D. Ramos, R. N. Sampaio, F. F. de Assis, K. T. de Oliveira, P. Homem-de-Mello, A. O. T. Patrocinio, K. P. M. Frin, *Dalton Trans.* **2016**, *45*, 11688.

[12] a) G. S. Huff, W. K. C. Lo, R. Horvath, J. O. Turner, X.-Z. Sun, G. R. Weal, H. J. Davidson, A. D. W. Kennedy, C. J. McAdam, J. D. Crowley, M. W. George, K. C. Gordon, *Inorg. Chem.* **2016**, *55*, 12238. b) G. E. Shillito, T. B. J. Hall, D. Preston, P. Traber, L. Wu, K. E. A. Reynolds, R. Horvath, X. Z. Sun, N. T. Lucas, J. D. Crowley, M. W. George, S. Kupfer, K. C. Gordon, *J. Am. Chem. Soc.* **2018**, *140*, 4534.

[13] H. van der Salm, M. G. Fraser, R. Horvath, J. O. Turner, G. M. Greetham, I. P. Clark, M. Towrie, N. T. Lucas, M. W. George, K. C. Gordon, *Inorg. Chem.* **2014**, *53*, 13049.

[14] K. S. Kisel, T. Eskelinen, W. Zafar, A. I. Solomatina, P. Hirva, E. V. Grachova, S. P. Tunik, I. O. Koshevoy, *Inorg. Chem.* **2018**, *57*(11), 6349.

[15] a) J. Wang, G. Hanan, *Synlett* **2005**, *2005*, 1251. b) Z. Yin, G. Zhang, T. Phoenix, S. Zheng, J. C. Fettinger, *RSC Adv.* **2015**, *5*, 36156. c) A. Maroń, A. Szlapa, T. Klemens, S. Kula, B. Machura, S. Krompiec, J. G. Małecki, A. Świtlicka-Olszewska, K. Erfurt, A. Chrobok, *Org. Biomol. Chem.* **2016**, *14*, 3793. d) A. Maroń, S. Kula, A. Szlapa-Kula, A. Świtlicka, B. Machura, S. Krompiec, *Eur. J. Org. Chem.* **2017**, *2017*, 2730.

[16] D. G. Vargas-Pineda, T. Guardado, F. Cervantes-Lee, A. J. Metta-Magana, K. H. Pannell, *Inorg Chem.* **2010**, *49*, 960.

[17] I. R. de Moraes, S. Scholz, M. Hermenau, M. L. Tietze, T. Schwab, S. Hofmann, M. C. Gather, K. Leo, *Org. Electron.* **2015**, *26*, 158.

[18] P. Bujak, I. Kulszewicz-Bajer, M. Zagorska, V. Maurel, I. Wielgus, A. Pron, *Chem. Soc. Rev.* **2013**, *42*, 8895.

[19] a) B. Laramee-Milette, C. Lachance-Brais, G. S. Hanan, *Dalton Trans.* **2015**, *44*, 41. b) C.-C. Ko, L. T.-L. Lo, C.-O. Ng, S.-M. Yiu, *Chem. Eur J.* **2010**, *16*, 13773. c) Q.-H. Wei, F.-N. Xiao, L.-J. Han, S.-L. Zeng, Y.-N. Duan, G.-N. Chen, *Dalton Trans.* **2011**, *40*, 5078. d) D. Wang, Q.-L. Xu, S. Zhang, H.-Y. Li, C.-C. Wang, T.-Y. Li, Y. M. Jing, W. Huang, Y. X. Zheng, G. Accorsi, *Dalton Trans.* **2013**, *42*, 2716. e) P. Gomez-Iglesias, F. Guyon, A. Khatyr, G. Ulrich, M. Knorr, J. M. Martin-Alvarez, D. Miguel, F. Villafane, *Dalton Trans.* **2015**, *44*, 17516.

[20] L. D. Ramos, R. N. Sampaio, F. F. de Assis, K. T. de Oliveira, P. Homem-de-Mello, A. O. T. Patrocinio, K. P. M. Frin, *Dalton Trans.* **2016**, *45*, 11688.

[21] a) S. Kim, T. K. An, J. Chen, I. Kang, S. H. Kang, D. S. Chung, C. E. Park, Y.-H. Kim, S.-K. Kwon, *Adv. Funct. Mater.* **2011**, *21*, 1616. b) Y. Zhang, L. Zhang, H. Liu, D. Sun, X. Li, *CrystEngComm* **2015**, *17*, 1453.

[22] M. J. Frisch, G. W. Trucks, H. B. Schlegel, G. E. Scuseria, M. A. Robb, J. R. Cheeseman, G. Scalmani, V. Barone, B. Mennucci, G. A. Petersson, H. Nakatsuji, M. Caricato, X. Li, H. P. Hratchian, A. F. Izmaylov, J. Bloino, G. Zheng, J. L. Sonnenberg, M. Hada, M. Ehara, K. Toyota, R. Fukuda, J. Hasegawa, M. Ishida, T. Nakajima, Y. Honda, O. Kitao, H. Nakai, T. Vreven, J. A. Montgomery Jr., J. E. Peralta, F. Ogliaro, M. J. Bearpark, J. Heyd, E. N. Brothers, K. N. Kudin, V. N. Staroverov, R. Kobayashi, J. Normand, K. Raghavachari, A. P. Rendell, J. C. Burant, S. S. Iyengar, J. Tomasi, M. Cossi, N. Rega, N. J. Millam, M. Klene, J. E. Knox, J. B. Cross, V. Bakken, C. Adamo, J. Jaramillo, R. Gomperts, R. E. Stratmann, O. Yazyev, A. J. Austin, R. Cammi, C. Pomelli, J. W. Ochterski, R. L. Martin, K. Morokuma, V. G. Zakrzewski, G. A. Voth, P. Salvador, J. J. Dannenberg, S. Dapprich, A. D. Daniels, Ö. Farkas, J. B. Foresman, J. V. Ortiz, J. Cioslowski, D. J. Fox, *Gaussian 09*, Gaussian Inc., Wallingford, CT, USA **2009**.

[23] T. Mutai, J. D. Cheon, S. Arita, K. Araki, *J. Chem. Soc. Perkin Trans. 2* **2001**, 1045.

[24] a G. Rajib, D. K. Palit, *J. Phys. Chem. A* **2015**, *119*, 11128. b G. Haberhauer, R. Gleiter, C. Burkhart, *Chem. Eur. J.* **2016**, *22*, 971. c G. Haberhauer, *Chem. Eur. J.* **2017**, *23*, 9288.

[25] M. Cocchi, J. Kalinowski, L. Murphy, J. A. G. Williams, V. Fattori, *Org. Electron.* **2010**, *11*, 388.

[26] a A. J. Lees, *Chem Rev.* **1987**, *87*, 711. b D. Wang, Q.-L. Xu, S. Zhang, H.-Y. Li, C.-C. Wang, T.-Y. Li, C. C. Wang, T. Y. Li, Y. M. Jing, W. Huang, Y. X. Zheng, G. Accorsi, *Dalton Trans.* **2013**, *42*, 2716.

[27] B. N. Ghosh, F. Topic, P. K. Sahoo, P. Mal, J. Linnera, E. Kalenius, H. M. Tuononen, K. Rissanen, *Dalton Trans.* **2015**, *44*, 254.

[28] a Q. Wu, T. Zhang, Q. Peng, D. Wang, Z. Shuai, *Phys. Chem. Chem. Phys.* **2014**, *16*, 5545. b T. Zhu, T. Van Voorhis, *J. Phys. Chem. C* **2016**, *120*, 19987. c K. Kotwica, P. Bujak, D. Wamil, A. Pieczonka, G. Wiosna-Salyga, P. A. Gunka, T. Jaroch, R. Nowakowski, B. Luszczynska, E. Witkowska, I. Glowacki, J. Ulanski, M. Zagorska, A. Pron, *J. Phys. Chem. C* **2015**, *119*, 10700. d S. Jenatsch, L. Wang, N. Leclaire, E. Hack, R. Steim, S. B. Anantharaman, J. Heier, B. Ruhstaller, L. Penninck, F. Nüesch, *Org. Electron.* **2017**, *48*, 77.

[29] a M. J. G. Peach, P. Benfield, T. Helgaker, D. J. Tozer, *J. Chem. Phys.* **2008**, *128*, 044118. b M. J. G. Peach, C. R. L. Sueur, K. Ruud, M. Guillaume, D. J. Tozer, *Phys. Chem. Chem. Phys.* **2009**, *11*, 4465. c J. Plötner, D. J. Tozer, A. Dreuw, J. Chem, *Theory Comput.* **2010**, *6*, 2315.

[30] Agilent Technologies, *CrysAlis CCD and CrysAlis RED*. Oxford Diffraction Ltd, Yarnton, Oxfordshire, UK **2012**.

[31] G. M. Sheldrick, *Acta Crystallogr. A* **2008**, *64*, 112.

[32] a) D. Andrae, U. Häußermann, M. Dolg, H. Stoll, H. Preuß, *Theor. Chim. Acta* **1990**, *77*, 123. b) F. Weigend, R. Ahlrichs, *Phys. Chem. Chem. Phys.* **2005**, *7*, 3297. c) D. Rappoport, F. Furche, *J. Chem. Phys.* **2010**, *133*, 134105.

[33] a) C. Adamo, V. Barone, *J. Chem. Phys.* **1999**, *110*, 6158. b) J. P. Perdew, K. Burke, M. Ernzerhof, *Phys. Rev. Lett.* **1996**, *77*, 3865.

[34] a) B. Mennucci, J. Tomasi, *J. Chem. Phys.* **1997**, *106*, 5151. b) E. Cancès, B. Mennucci, J. Tomasi, *J. Chem. Phys.* **1997**, *107*, 3032. c) M. Cossi, V. Barone, B. Mennucci, J. Tomasi, *Chem. Phys. Lett.* **1998**, *286*, 253.

[35] a) M. W. Schmidt, K. K. Baldridge, J. A. Boatz, S. T. Elbert, M. S. Gordon, J. H. Jensen, S. Koseki, N. Matsunaga, K. A. Nguyen, S. Su, T. L. Windus, M. Dupuis, J. A. Montgomery, *J. Comput. Chem.* **1993**, *14*, 1347. b) M. S. Gordon, M. W. Schmidt, *Theory and Applications of Computational Chemistry*, Elsevier **2005** 1167.

[36] A. V. Marenich, C. J. Cramer, D. G. Truhlar, *J. Phys. Chem. B* **2009**, *113*, 6378.

[37] a) B. O. Roos, in *Lecture Notes in Quantum Chemistry*, (Ed: B. O. Roos) Vol. 58, Springer, Berlin **1992** 177. b) B. O. Roos, in *Advances in Chemical Physics*, (Ed: K. P. Lawley) Vol. 69, John Wiley & Sons, Inc., Hoboken, NJ, USA **1987** 399.

[38] a) K. Andersson, P. A. Malmqvist, B. O. Roos, A. J. Sadlej, K. Wolinski, *J. Phys. Chem.* **1990**, *94*, 5483. b) J. Finley, P.-Å. Malmqvist, B. O. Roos, L. Serrano-Andrés, *Chem. Phys. Lett.* **1998**, *288*, 299.

[39] a)G. Karlström, R. Lindh, P.-Å. Malmqvist, B. O. Roos, U. Ryde, V. Veryazov, P.-O. Widmark, M. Cossi, B. Schimmelpfennig, P. Neogrady, L. Seijo, *Comput. Mater. Sci.* **2003**, *28*, 222. b)V. Veryazov, P. O. Widmark, L. Serrano-Andrés, R. Lindh, B. O. Roos, *Int. J. Quantum Chem.* **2004**, *100*, 626. c)F. Aquilante, L. De Vico, N. Ferré, G. Ghigo, P.-Å. Malmqvist, P. Neogrády, T. B. Pedersen, M. Pitonak, M. Reiher, B. O. Roos, L. Serrano-Andrés, M. Urban, V. Veryazov, R. Lindh, *J. Comput. Chem.* **2010**, *31*, 224. d) The following persons have contributed to the development of the Molcas software: K. Andersson, F. Aquilante, M. Barysz, A. Bernhardsson, M. R.A. Blomberg, J. Boström, Y. Carissan, L. Chibotaru, D. L. Cooper, M. Cossi, M. Delcey, A. Devarajan, L. De Vico, I. F. Galván, N. Ferré, M. P. Fülscher, A. Gaenko, L. Gagliardi, G. Ghigo, C. de Graaf, S. Gusarov, B. A. Hess, D. Hagberg, J. M. Hermida-Ramón, A. Holt, G. Karlström, J. W. Krogh, R. Lindh, P.-Å. Malmqvist, T. Nakajima, P. Neogrády, J. Olsen, T. B. Pedersen, D. Peng, M. Pitonak, J. Raab, M. Reiher, B. O. Roos, U. Ryde, B. Schimmelpfennig, M. Schütz, L. Seijo, L. Serrano-Andrés, I. Schapiro, P. E. M. Siegbahn, J. Stålring, B. Suo, P. Sushko, T. Thorsteinsson, T. Tsuchiya, L. Ungur, S. Vancoillie, V. Veryazov, V. Vysotskiy, P.-O. Widmark.

[40] a) P.-O. Widmark, P.-Å. Malmqvist, B. O. Roos, *Theor. Chim. Acta* **1990**, *77*, 291. b) P.-O. Widmark, B. J. Persson, B. O. Roos, *Theor. Chim. Acta* **1991**, *79*, 419.

SUPPORTING INFORMATION

Additional supporting information may be found online in the Supporting Information section at the end of the article.

How to cite this article: Klemens T, Świtlicka A, Szlapa-Kula A, et al. Experimental and computational exploration of photophysical and electroluminescent properties of modified 2,2′:6′,2″-terpyridine, 2,6-di(thiazol-2-yl)pyridine and 2,6-di(pyrazin-2-yl)pyridine ligands and their Re(I) complexes. *Appl Organometal Chem*. 2018; e4611. https://doi.org/10.1002/aoc.4611